Two-Day Disturbances in the Tropical Western Pacific

by

Patrick T. Haertel

Department of Atmospheric Science
Colorado State University
Fort Collins, Colorado

Colorado State University

Department of Atmospheric Science

Paper No. 589

TWO-DAY DISTURBANCES IN THE TROPICAL

WESTERN PACIFIC

by

Patrick T. Haertel

Department of Atmospheric Science
Colorado State University
Fort Collins, CO 80523

Fall 1995

ABSTRACT

TWO-DAY DISTURBANCES IN THE TROPICAL WESTERN PACIFIC

From November 1992 through February 1993, westward-propagating disturbances frequented the equatorial western Pacific. They had a scale of about 1000 km and propagated at about 16 m s^{-1}. Locally, their passage was accompanied by a two-day oscillation in high cloudiness. I investigate the kinematic and thermodynamic structure of these two-day disturbances using composites of surface, satellite and sounding data. The disturbances propagated westward at about 14 m s^{-1} faster than the mean tropospheric flow, apparently through a dynamical mechanism. Numerical simulations, supported by time-pressure series of wind, shed light on this dynamical mechanism. A heat source whose vertical profile is that of the 2-day disturbances' convection excites two internal modes that combine to create an environment favorable for convection to the west of the heat source. The essence of the 2-day disturbance is apparently a coupling between convection and these two modes.

ACKNOWLEDGMENTS

TABLE OF CONTENTS

LIST OF FIGURES

Chapter 1

INTRODUCTION

The surface of the open oceans is warmest near the equator from the Maritime Continent to just east of the dateline. This region is referred to as the western Pacific 'warm pool.' Moist convection produces more rainfall and releases more latent heat over the warm pool than in any other region of the world. Understanding the organization of this convection and how it couples with oceanic processes is a step towards more accurate seasonal and long term forecasts for the entire planet (Webster and Lukas, 1992). This paper aims to further such an understanding by studying a particular convective feature of the warm pool--the two-day disturbance. Before discussing what is already known about the two-day disturbance, I will provide a brief overview of convective organization over the warm pool.

Warm pool convection is often organized within a hierarchy of systems (Nakazawa 1988, 1995; Hendon and Liebmann, 1994). The Intraseasonal Oscillation (ISO) tops this hierarchy. The ISO is a region of enhanced convection with a longitudinal width on the order of 90° which moves eastward along the equator across the Indian and western Pacific oceans (Hendon and Liebmann, 1994). Locally the passage of the ISO is accompanied by a 40-50 day oscillation in surface pressure, lower-level and upper-level winds, and mean tropospheric temperature (see review by Madden and Julian, 1994).

The ISO's convection is further organized into a series of eastward-propagating disturbances named 'super clusters' by Nakazawa (1988). Each super cluster is several

thousand kilometers across and moves eastward at 10-15 m s^{-1}. Super clusters also have a fine structure. Each typically consists of a series of westward-propagating disturbances with a period of about 2 days. These two-day disturbances are the focus of this paper. The super cluster propagates eastward as 2-day disturbances develop on its eastern edge and diminish on its western edge (Nakazawa 1988).

Two-day disturbances have previously been studied primarily with satellite data. In one such study, Hendon and Liebmann (1994) created a composite time-longitude series of the 2-day disturbance using high-resolution global cloud imagery from 1 November 1987 to 31 May 1988. The composite disturbance had a longitudinal wavelength of about 2000 km, and it propagated westward at 15 m s^{-1}. They speculated that the disturbances which made up their composite were either long-lived squall lines or cloud clusters that were advected westward by mean tropospheric easterlies. They suggested that these disturbances did not play an active role in the evolution of the ISO, but responded to the large-scale forcing of the ISO.

Takayabu (1994) studied 2-day disturbances using ten years of infrared brightness temperature data from the Japanese Geostationary Meteorological Satellite. She found that 2-day disturbances were most common from December to February within 8° latitude of the equator. She created a composite satellite view of 263 2-day disturbances which occurred during the months December, January, February from 1980 to 1989. The composite disturbance appeared as an area of high cloudiness nearly 1000 kilometers across which moved westward along the equator at 19 m s^{-1} and dispersed in an arc. She found that the disturbance's cloud pattern and its propagation resembled an $n = 1$ inertio-gravity wave (predicted by Matsuno, 1966) with an equivalent depth of about 20 m. Although she did not provide a physical explanation for this equivalent depth, she did provide such an explanation for the 2-day period. She referred to modeling work by Sarachik (1985) which suggest that the atmosphere below the trade inversion recovers from convection in about 2 days.

2

Chen et al (1995) studied the 2-day disturbances which occurred during the Tropical Ocean-Global Atmosphere Coupled Ocean-Atmosphere Response Experiment (TOGA COARE). By using a computer program to identify and track individual cloud clusters, they found that most 2-day disturbances consisted of many cloud clusters moving in various directions with favored development of new clusters towards the west. They estimated the rate of disturbance propagation to be 10-15 m s^{-1} and speculated that internal gravity waves played a role in this propagation.

Although the kinematic and thermodynamic structure of 2-day disturbances has not been observed in situ, Lau et al (1989) simulated these disturbances with a numerical model. In the beginning of their simulation of the ISO, westward-propagating disturbances developed within eastward moving 'super clusters'. These disturbances propagated at about 16 m s^{-1} and resembled the mixed Rossby-gravity wave (Matsuno, 1966) in wind structure. Later in the simulation these disturbances were absent, however; convection was only organized on larger scales.

Despite these studies of 2-day disturbances a number of questions remain. How do they propagate? Does their convection couple with mixed Rossby-gravity waves (Lau, 1989) or inertio-gravity waves (Takayabu, 1994), or are they long-lived squall lines or cloud clusters which are advected westward (Hendon and Liebmann, 1994)? Why do they have a two-day period? Does the lower atmosphere take 2 days to recover from deep convection (Takayabu, 1994), or is there a dynamical explanation for the 2-day period? What is the nature of the convection which accompanies the 2-day disturbance? The purpose of·this paper is to answer these questions. In order to accomplish this goal I use satellite, surface, and sounding observations collected within TOGA COARE, and a numerical model.

Chapter 2

DATA AND METHODS

2.1 Sounding and Surface Observations

The sounding and surface observations presented in this study were collected within the Tropical Ocean-Global Atmosphere Coupled Ocean-Atmosphere Response Experiment (TOGA COARE). This experiment was designed to study the interaction between atmospheric and oceanic processes over the western Pacific warm pool. During the Intensive Operating Period (IOP) of TOGA COARE, which was from November 1992 through February 1993, almost 1200 people from more than 20 nations joined forces to launch 12,000 rawinsondes, maintain 30 moorings, operate 14 ships, and complete 125 aircraft flights.

The sounding data were collected at an array of six stations called the Intensive Flux Array (IFA) (Figure 2.1). At these stations rawinsondes were released every six hours for most of the IOP. The rawinsondes measured pressure, temperature, and humidity and their position was tracked in order to measure wind. Four of the six IFA sounding stations were on ships and the other two, Kavieng and Kapingamarangi, were on islands. To acquire mean vertical profiles for the IFA the sounding data was first linearly interpolated to the pressure levels 100 kPa, 97.5 kPa, 95 kPa, . . . 10 kPa, and then averaged over all reporting stations.

The vertical heating profile of the two-day disturbance (Figure 3.1) was derived from 18 profiles of IFA ω (pressure velocity) that were donated by Xin Lin of Colorado State University (see Lin and Johnson, 1995 for a discussion of how ω was calculated).
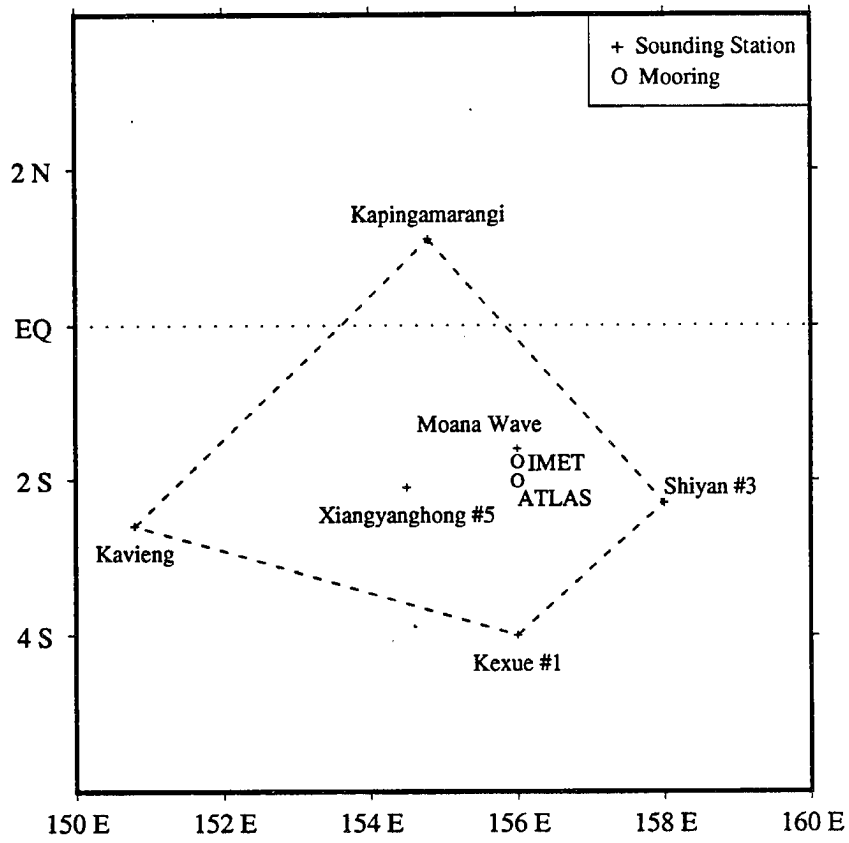
Figure 2.1: TOGA COARE Intensive Flux Array (IFA). The locations of the ships Xiangyanghong #5, Shiyan #3, Moana Wave, and Kexue #1, and the IMET and ATLAS moorings varied slightly from day to day.

Each ω profile was measured within six hours of when a two-day disturbance was centered over the IFA. The 18 profiles were averaged and then heating Q was approximated using the following equation:

$$Q = \omega \, \frac{T \, \partial log(\theta)}{\partial p} \tag{2.1}$$

where T denotes temperature, p pressure, and θ equivalent potential temperature. Equation (2.1) is based on the premise that the adiabatic cooling/warming associated with vertical motion balances convective heating/cooling for the spatial scale of the IFA and the time scale of 6 hours.

The calculations of Convective Available Potential Energy (Moncrieff and Miller, 1976) and Convective Inhibition (Colby 1984) shown in Figure 4.24 were made from IFA mean profiles of temperature and humidity. I assumed that the rising air parcel originated from 97.5 kPa and that all condensed water fell out of the parcel. Both the parcel's temperature and mixing ratio were taken into account in the calculation of parcel density. Convective Inhibition was integrated from 97.5 kPa to the level were the parcel's density equaled the environment's density.

The surface measurements presented in this paper were recorded primarily by the IMET mooring (Figure 2.1), which was operated by the Woods Hole Oceanographic Institution. This buoy measured surface wind, temperature, pressure, humidity, sea surface temperature, rainfall and many other variables. The sea surface temperature measurements were made at a depth of 0.45 m, and the rain rate measurements were 24-hour block averages of data from the IMET buoy, the ATLAS buoy, and the ships Wecoma and Moana Wave.

2.2 Satellite Data

The Geostationary Meteorological Satellite provided the infrared brightness temperature data used in this study. The pictures used in case studies have a resolution of one-tenth degree latitude/longitude. The shading of brightness temperatures in these frames is as follows: white denotes values below 208 K, light gray denotes values between 208 K and 235 K, dark gray denotes values between 235 K and 278 K, and black denotes values greater than 278 K.

Some of the satellite data presented in Chapter 4 (Figures 4.2 and 4.3) were filtered with a bandpass filter. The filter was designed to select Fourier components with periods between 1.6 and 3.0 days. It is based on a weighting function of the form $\frac{sin(mt) - sin(nt)}{t}$, where m and n are the highest and lowest frequencies selected. The width of the weighting function was 18 days, and Figure 2.2 shows that it serves its purpose.
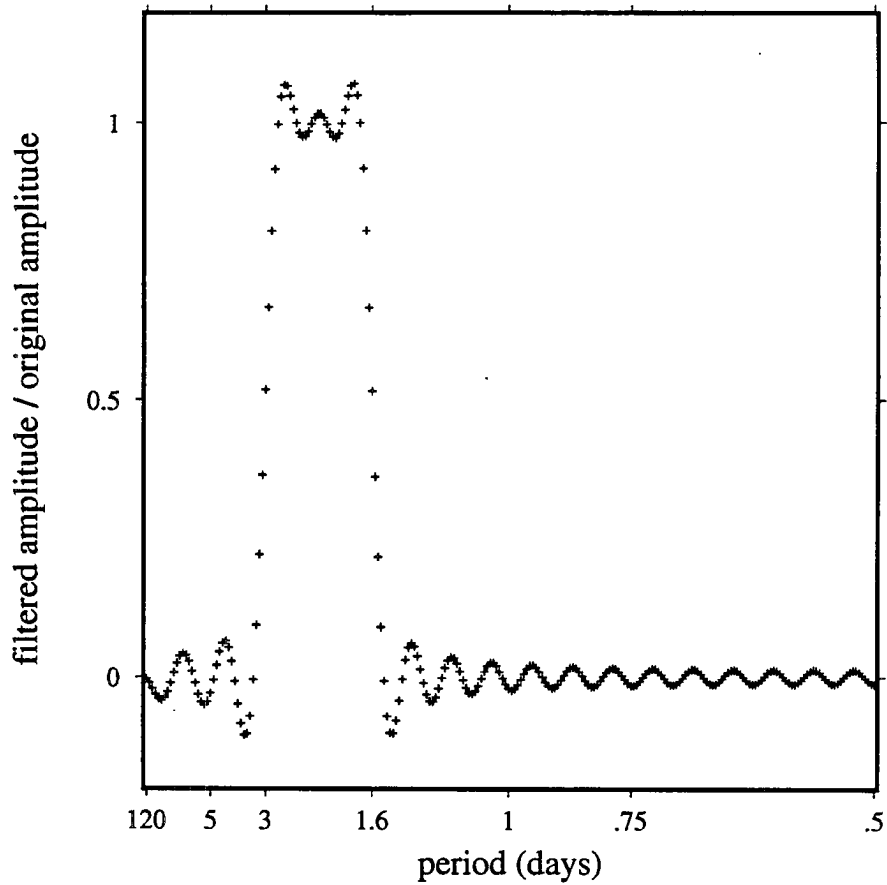
Figure 2.2: The effect of the bandpass filter on Fourier components with periods of .5 to 120 days. The goal is to preserve oscillations with periods of 1.6 to 3 days while removing all others.

Chapter 3

THE COMPUTER MODEL

3.1 Model Equations

The computer model is based on the following differential equations:

$$\frac{\partial u}{\partial t} - \beta y v + \frac{\partial \phi}{\partial x} = 0 \tag{3.1}$$

$$\frac{\partial v}{\partial t} + \beta y u + \frac{\partial \phi}{\partial y} = 0 \tag{3.2}$$

$$\frac{\partial T}{\partial t} - S_p\, \omega = Q \tag{3.3}$$

$$\omega = - \int_{p_T}^{p} (\frac{\partial u}{\partial x} + \frac{\partial v}{\partial y})\, dp \tag{3.4}$$

$$\phi = \int_{p_T}^{p} -\frac{RT}{p}\, dp - \frac{1}{p_B - p_T} \int_{p_T}^{p_B} (\int_{p_T}^{p'} -\frac{RT}{p}\, dp')\, dp \tag{3.5}$$

where p is pressure, p_T = 10 kPa, p_B = 100 kPa, u is zonal velocity, v is meridional

velocity, t is time, $\beta = \dfrac{\partial f}{\partial y}$, f is the Coriolis parameter, T is perturbation temperature, R

is the gas constant for dry air, ϕ is perturbation geopotential, ω is the Lagrangian

derivative of pressure, $S_p = -T\, \dfrac{\partial \log \theta}{\partial p}$, θ is potential temperature, and Q is heating.

9

Equations (3.1 - 3.5) are a linearized version of the primitive equations. Equations 3.1 and 3.2 are the momentum equations, equation 3.3 is the thermodynamic energy equation, equation 3.4 is derived from the continuity equation and the boundary condition $\omega(p_T) = 0$, and equation 3.5 is derived from the hydrostatic equation and the condition that $\int_{p_T}^{p_B} \phi \, dp = 0$, which is included to filter out the external mode. Fulton and Schubert (1985) discuss the theoretical solutions of these equations.

3.2 Finite Differencing

The system of partial differential equations (3.1-3.5) is solved on a grid with 19 pressure levels and a 31 point width in each horizontal direction. The horizontal resolution is 233 km and the vertical resolution is 5 kPa. Time derivatives are evaluated with the leapfrog method, and spatial derivatives are evaluated according to a fourth order Taylor series method.

Error magnitude depends both on the grid-spacing and the time-step. To select values for each, numerous test simulations were made. The solutions were stable when the time-step was equal to half the time required for the fastest mode to cross the horizontal grid-spacing. The stable test simulations were compared with the modeling results of Mapes and Houze (1995) and found to be compatible.

3.3 Heat Source

The vertical profile of the heat source used in the model (Figure 3.1) was measured with sounding data. The heat source is centered on the equator, and its horizontal structure resembles the positive part of a sine wave and has a 600 km radius. This scale was selected to match the scale of the composite disturbance as observed by satellite (Figure 4.20).

10

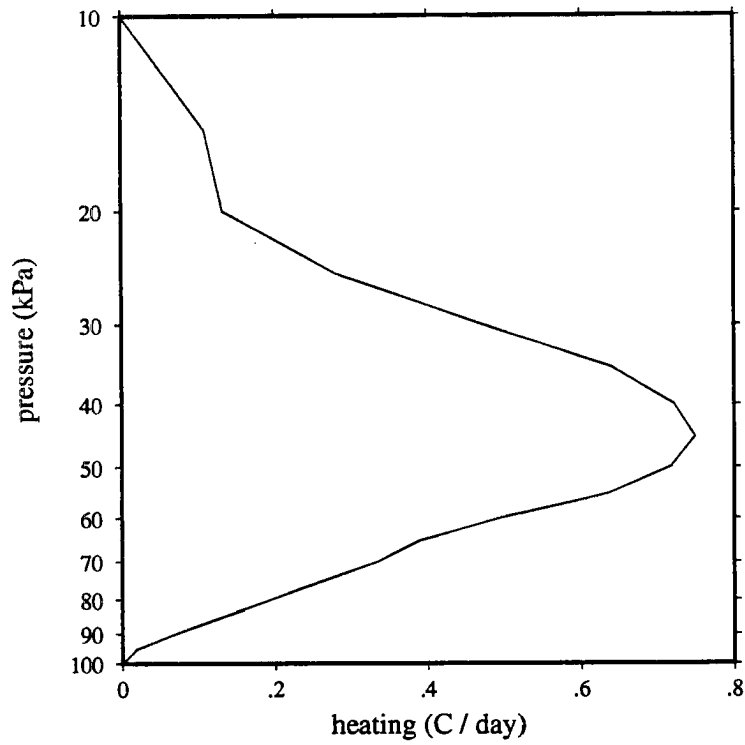Figure 3.1: The vertical profile of heating (°C hour^{-1}) associated with the two-day disturbances that passed over the IFA during the IOP. The 18 omega profiles used to calculate the heating function were provided by Xin Lin of Colorado State University.

Chapter 4

OBSERVATIONS OF TWO-DAY DISTURBANCES

This chapter contains satellite, surface, and sounding observations of the COARE two-day disturbances. Their climatology, convective character, thermodynamic structure, and kinematic structure are discussed.

4.1 Spectral Analysis of Brightness Temperature

Since a two-day oscillation in cloudiness accompanies the passage of a two-day disturbance, a good measure of two-day disturbances' frequency and intensity is the amplitude of Fourier components of brightness temperature with periods of about two-days. In this section, measurements of these components for the COARE IOP are presented in order to address three questions: (1) what percentage of the warm pool's convection is associated with two-day disturbances, (2) when are two-day disturbances most common, and (3) where are they most common?

Figure 4.1 assesses the two-day disturbance's contribution to IFA convection. It is a plot of the Fourier components of IFA brightness temperature during the IOP. They have been weighted by frequency and plotted as a function of the logarithm of frequency, so that the variance in brightness temperature associated with a particular peak is proportional to the area under that peak. Oscillations on four different time scales contributed most of the variance during the period. These are the 60-day, 13-day, 5-day, and 2-day oscillations. The 60-day oscillation has been extensively studied (Madden and Julian, 1994). The 13-day oscillation may be a signal of the super clusters noted by
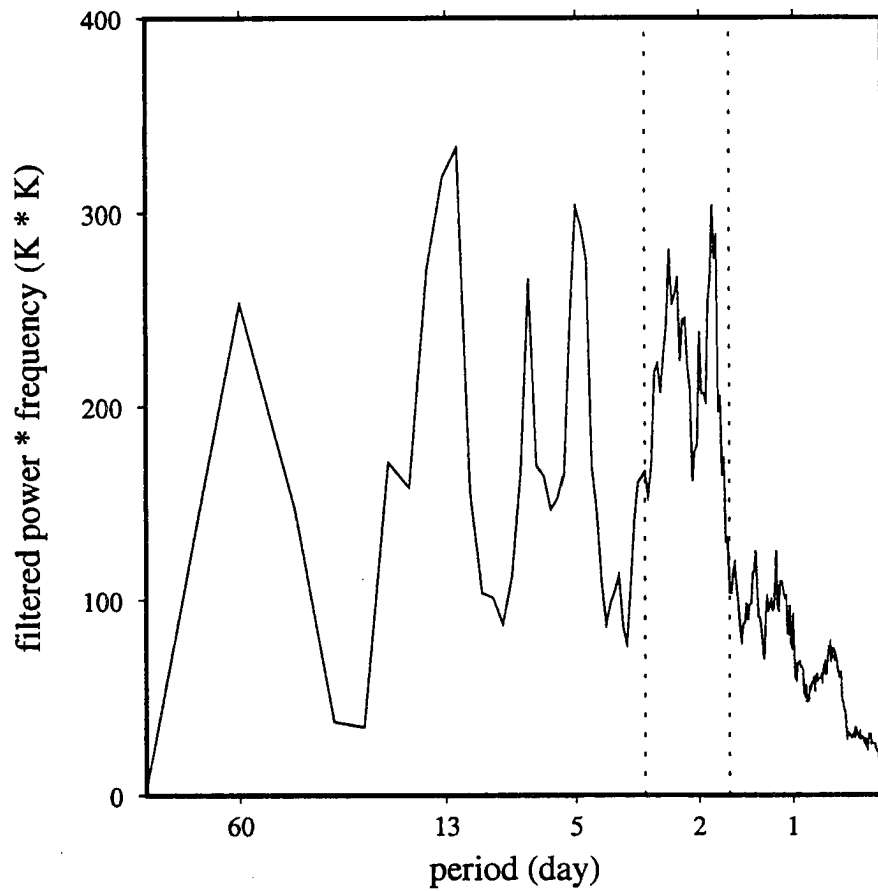
Figure 4.1: Fourier Analysis of IFA brightness temperature during the IOP. The dotted

lines correspond to periods of 1.6 and 3.0 days.

13

Nakazawa (1988). Numaguti et al (1995) associated the 5-day oscillation with mixed Rossby-gravity waves. The disturbances responsible for the two-day oscillation are of course the focus of this paper. They contributed about one-sixth of the IFA brightness temperature variance. Takayabu (1994) found the spectral signal of two-day disturbances to be even more pronounced in the boreal winters of 1982-1983 and 1986-1987.

During the IOP, two-day components of IFA brightness temperature oscillated with the greatest amplitude in December (Figure 4.2). At times during this month there was a 60° C swing in the IFA filtered brightness temperature from one day to the next. There were also active periods in late November, late January, and mid February. The amplitude of two-day components was apparently enhanced by the two intraseasonal oscillations which occurred in December and late January (Nakazawa 1995). Hendon and Liebmann (1994) and Nakazawa (1995) previously documented the connection between two-day disturbances and the intraseasonal oscillation.

Two-day disturbances preferentially occurred near the equator between 140° and 170° E. In that region two-day components accounted for one-fifth of the total brightness temperature variance (Figure 4.3). One interpretation of this pattern is that two-day disturbances typically form around 170° E and then propagate westward along the equator before dissipating around 140° E. Using satellite data from 1981 to 1989, Takayabu (1994) also noted that two-day disturbances are most common near the equator.

4.2 Case Studies

The purpose of this section is to acquaint the reader with the horizontal structure and movement of two-day disturbances, and to show that advection usually cannot explain their movement. Satellite pictures and wind profiles of six two-day disturbances which passed over the IFA during the IOP are presented. Each disturbance discussed here met two criteria. First, it was a large scale disturbance (~1000 km) which moved over the IFA. Second, the filtered IFA brightness temperature (Figure 4.2) fell below
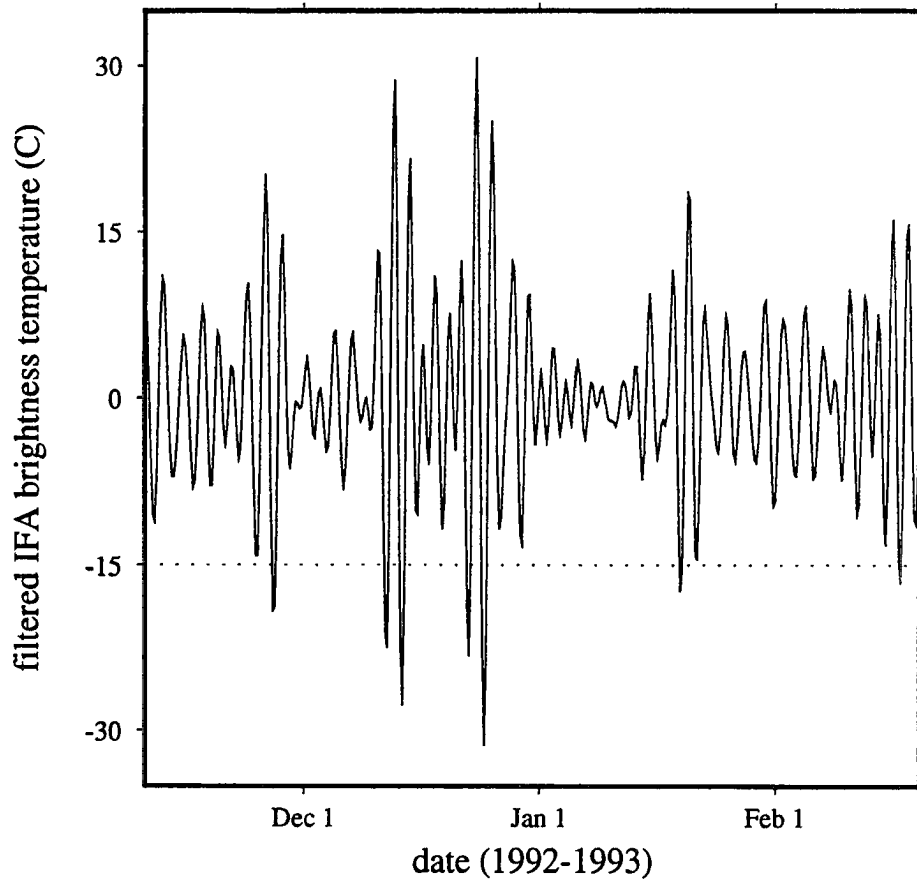
14

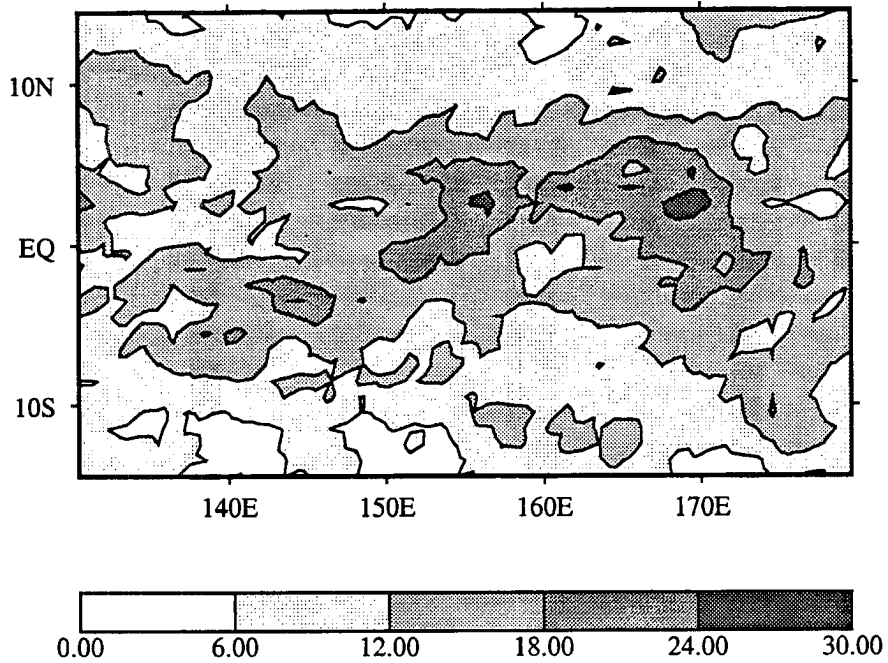Figure 4.2: Filtered IFA brightness temperature--only 1.6 to 3-day Fourier components remain.

Figure 4.3: The relative variance of 1.6 to 3-day oscillations over the western Pacific during the period 11 November 1992 to 19 February 1993. The percentage of total variance associated with such oscillations is contoured.

− 15°C during disturbance passage.

The first two-day disturbance passed over the IFA on 27 November 1992 (Figure 4.4). It appeared as a large area of high cloudiness which moved towards the southwest. The disturbance was most intense from 06Z 26 November through 18Z 26 November when the 208 K cloud tops (shaded white) covered the greatest area. During this time, the lowest brightness temperatures propagated towards the southwest at about 8 m s^{-1}. After 18Z 26 November 1992 cloudiness spread more rapidly to the southwest. During the two-day period covered by the satellite frames, the IFA wind profile had weak southwesterlies from the surface to 70 kPa, easterlies of 8 m s^{-1} from 60 to 20 kPa, and northeasterlies of 8-16 m s^{-1} above 20 kPa (Figure 4.5).

The second two-day disturbance passed over the IFA on 12 December 1992 (Figure 4.6). It appeared as a region of high cloudiness more than 1000 km across which consisted of multiple cloud clusters at times. Although the movement of individual clusters was variable, the system as a whole moved westward at about 14 m s^{-1}. There was little wind below 80 kPa and and easterlies and northeasterlies of 0 – 8 m s^{-1} between 80 and 20 kPa (Figure 4.7).

The third two-day disturbance hit the IFA on 14 December 1992. A cloud cluster developed over the IFA and then moved west-northwest at about 8 m s^{-1} (Figure 4.8). Between 00Z and 06Z on 14 December the lowest brightness temperatures spread northward. After 06Z 14 December they spread mainly westward. The wind profile for this case shows weak northerlies below 70 kPa and east-northeasterlies of 2-8 m s^{-1} from 70 to 20 kPa (Figure 4.9).

The fourth two-day disturbance passed over the IFA at 18Z on 22 December 1992. It consisted of many short-lived cloud clusters which moved in many directions (Figure 4.10). The system as a whole moved westward at around 14 m s^{-1}. The IFA wind profile included westerlies of 5-10 m s^{-1} below 60 kPa, nearly no wind from 60 to 30 kPa, and

06Z 26 November 92

06Z 27 November 1992

12Z 26 November 1992

12Z 27 November 1992

18Z 26 November 1992

18Z 27 November 1992

00Z 27 November 1992
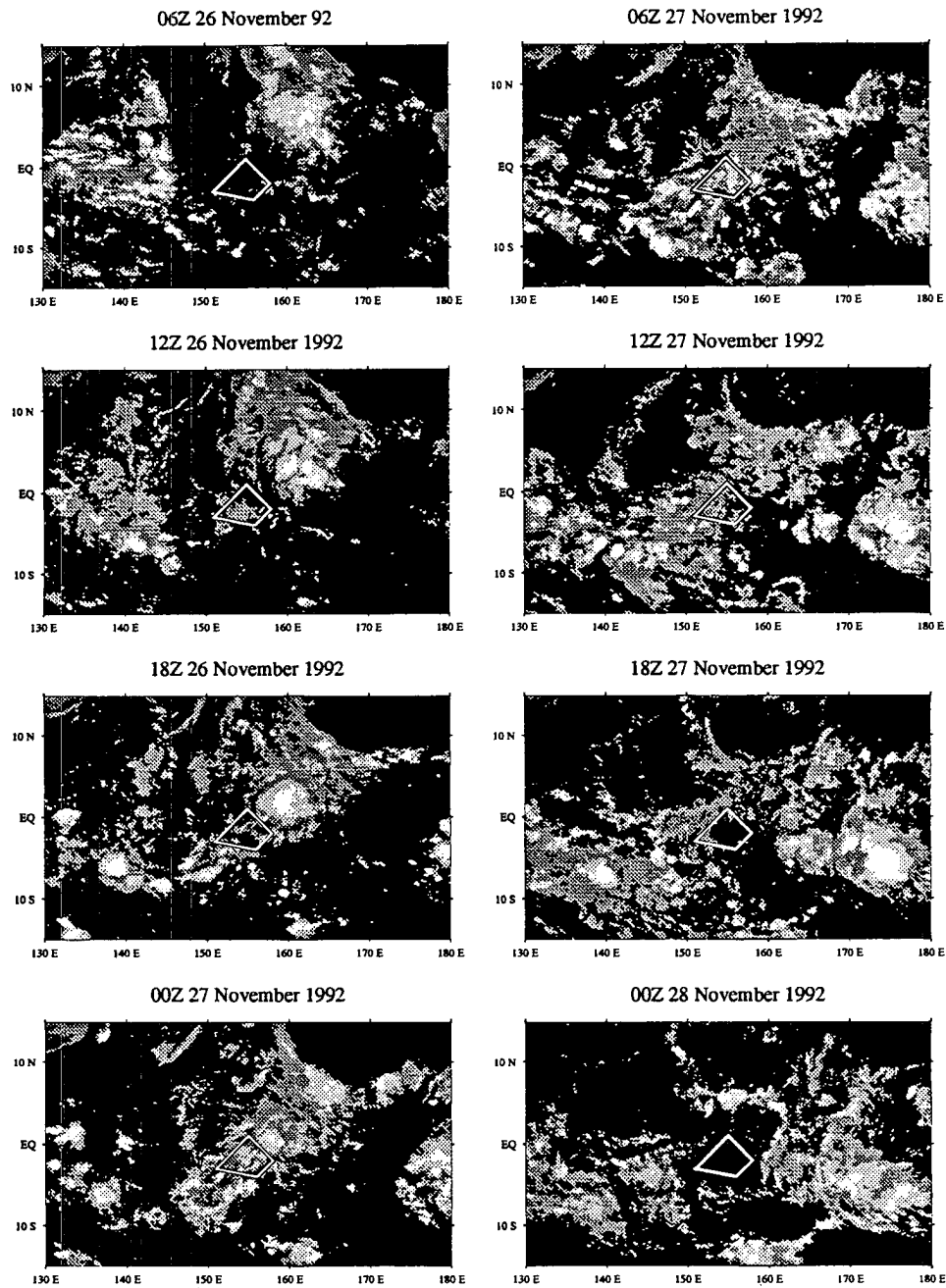
00Z 28 November 1992

Figure 4.4: Infrared satellite view of the 27 November 1992 case. See Chapter 2 for a discussion of the shading scheme. The IFA is outlined.
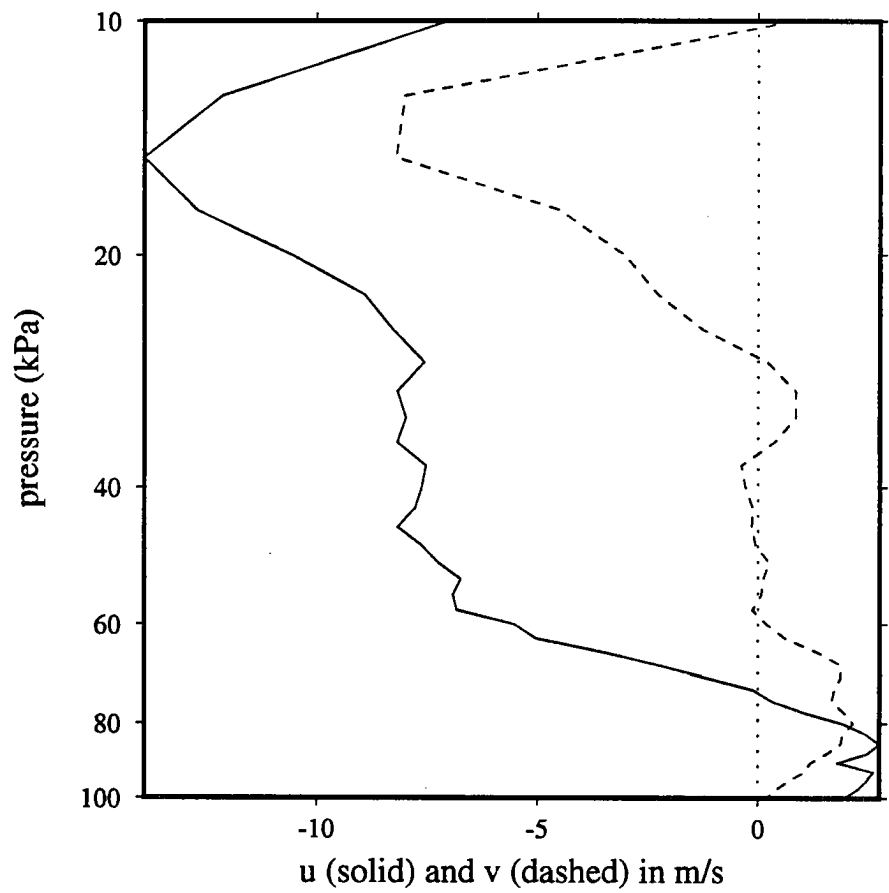
18

Figure 4.5: IFA mean wind profile for 00Z 26 November 1992 through 00Z 28 November 1992.

06Z 11 December 1992 **06Z 12 December 1992**

12Z 11 December 1992 **12Z 12 December 1992**

18Z 11 December 1992 **18Z 12 December 1992**

00Z 12 December 1992 **00Z 13 December 1992**

Figure 4.6: Infrared satellite view of the 12 December 1992 case. The IFA is outlined.

Figure 4.7: IFA mean wind profile for 00Z 11 December 1992 through 00Z 13 December 1993.
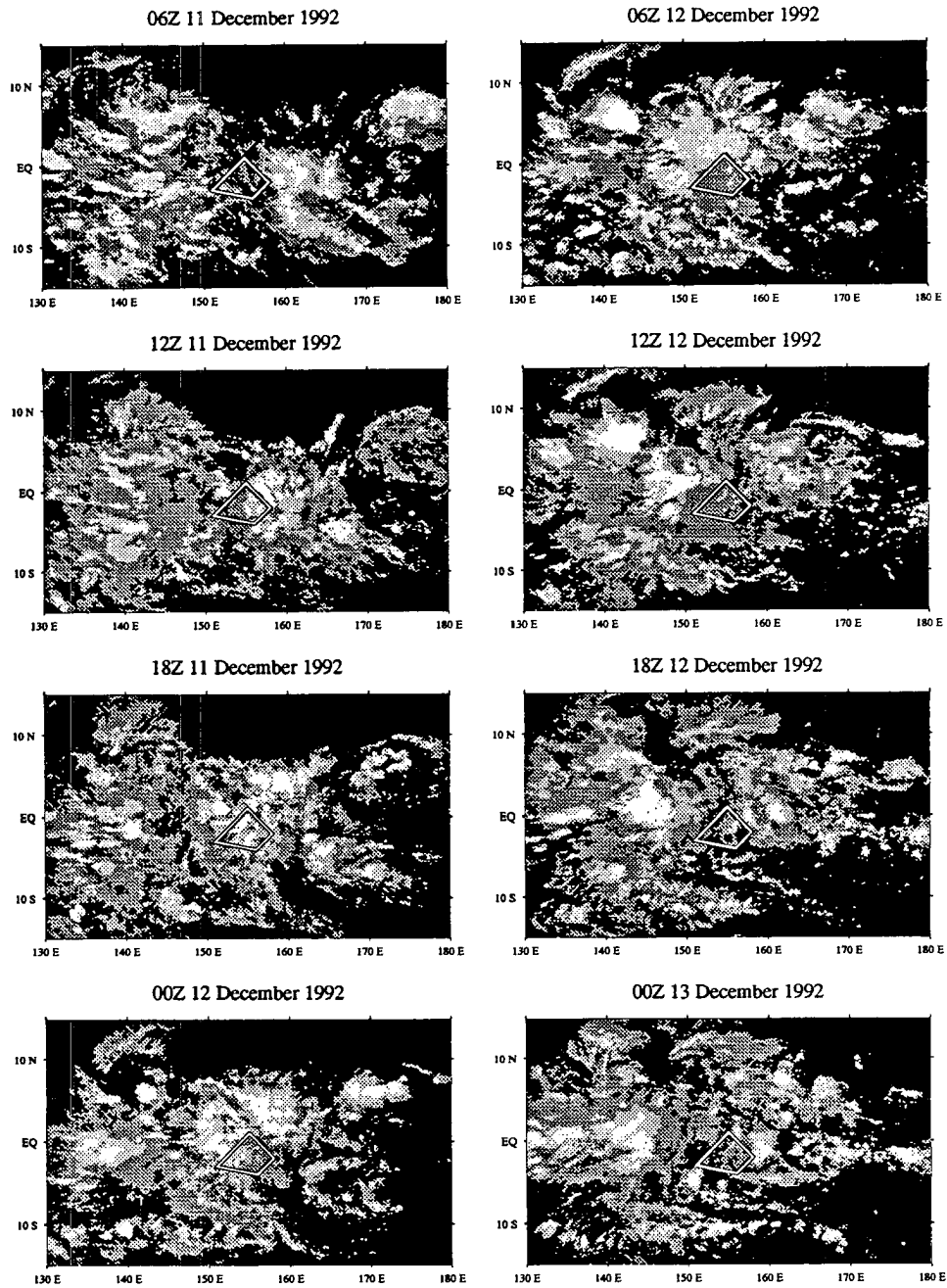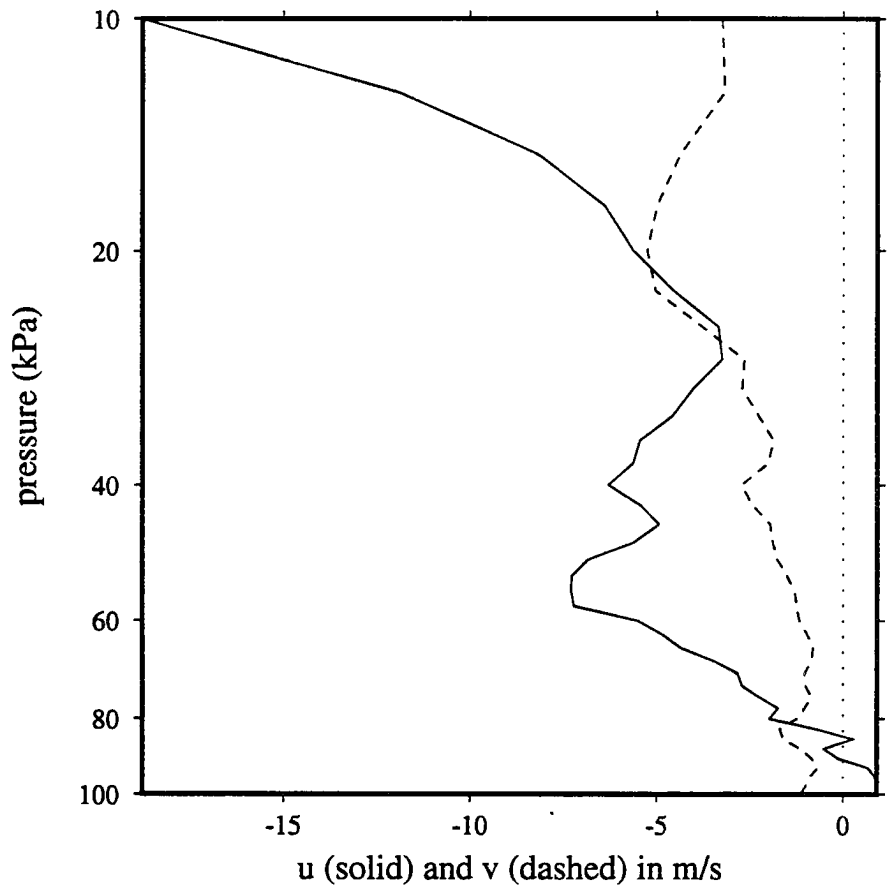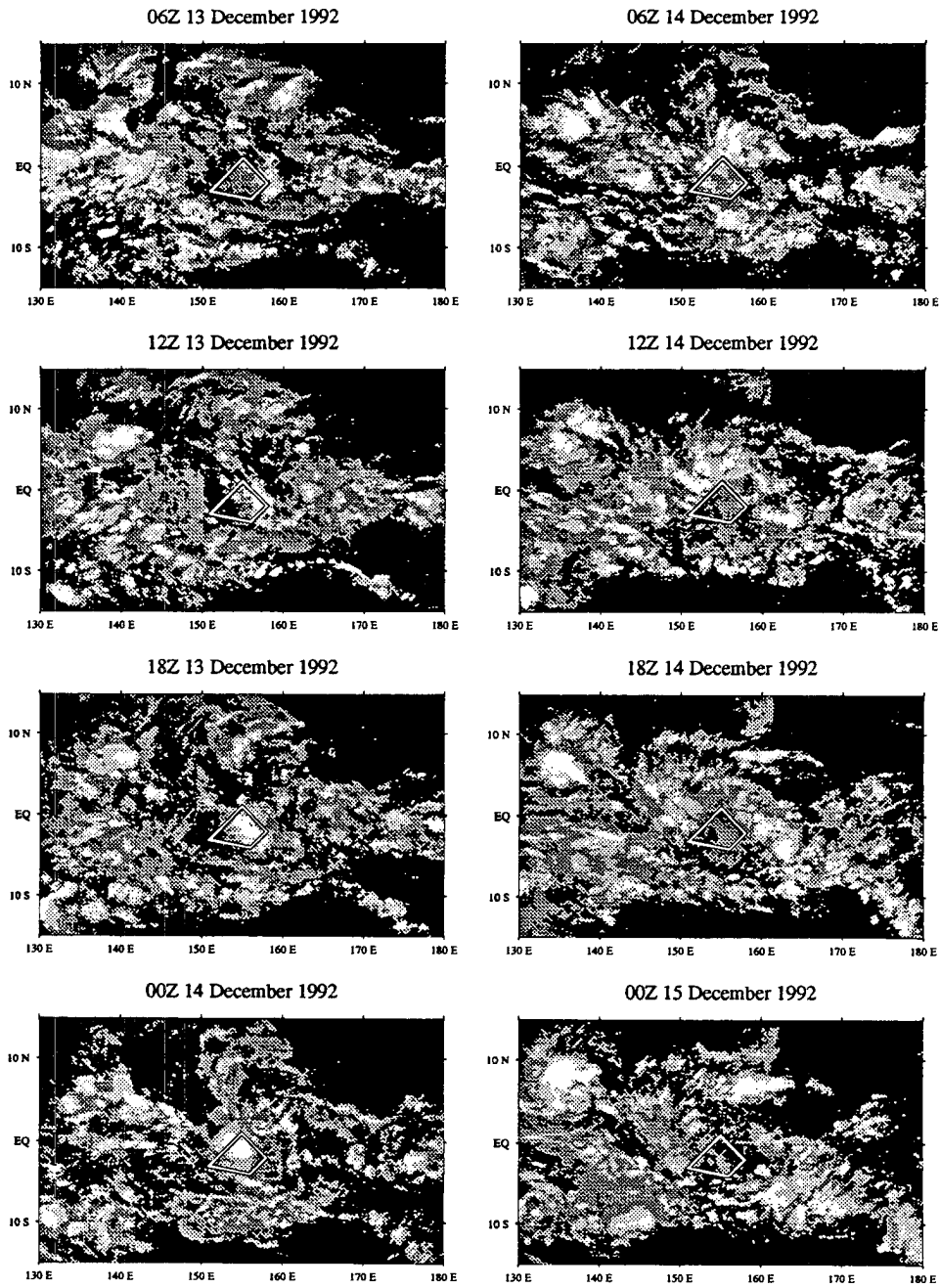
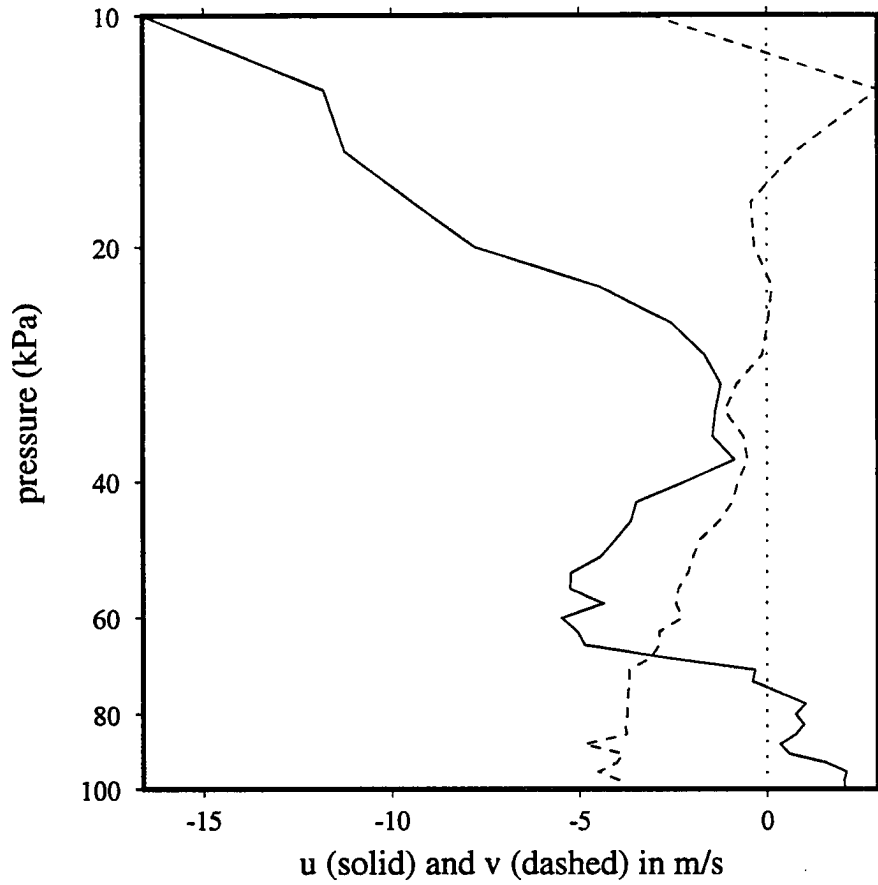Figure 4.8: Infrared satellite view of the 14 December 1992 case. The IFA is outlined.

Figure 4.9: IFA mean wind profile for 00Z 13 December 1992 through 00Z 15 December 1992.
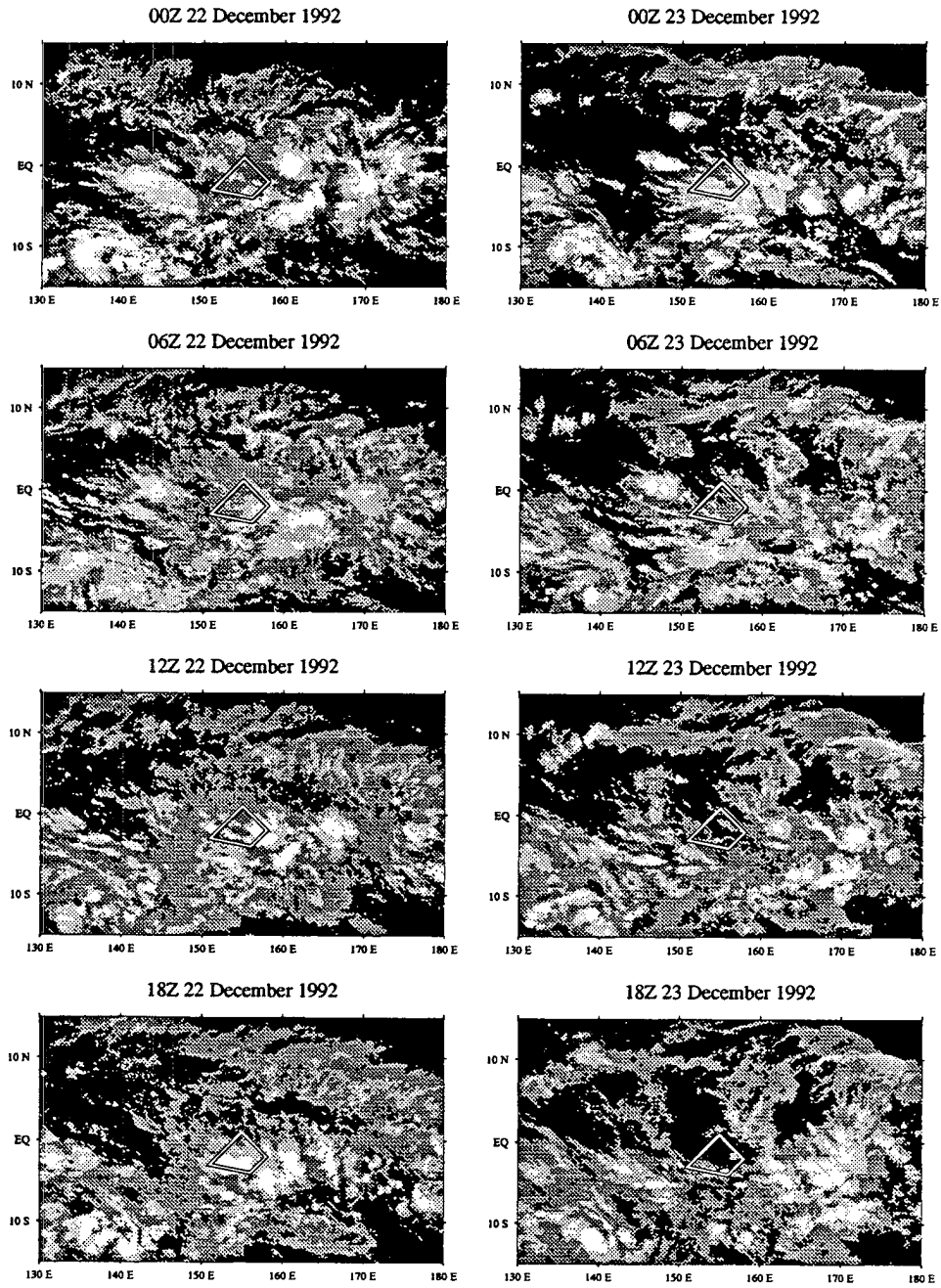
Figure 4.10: Infrared satellite view of 22 December 1992 case. The IFA is outlined.
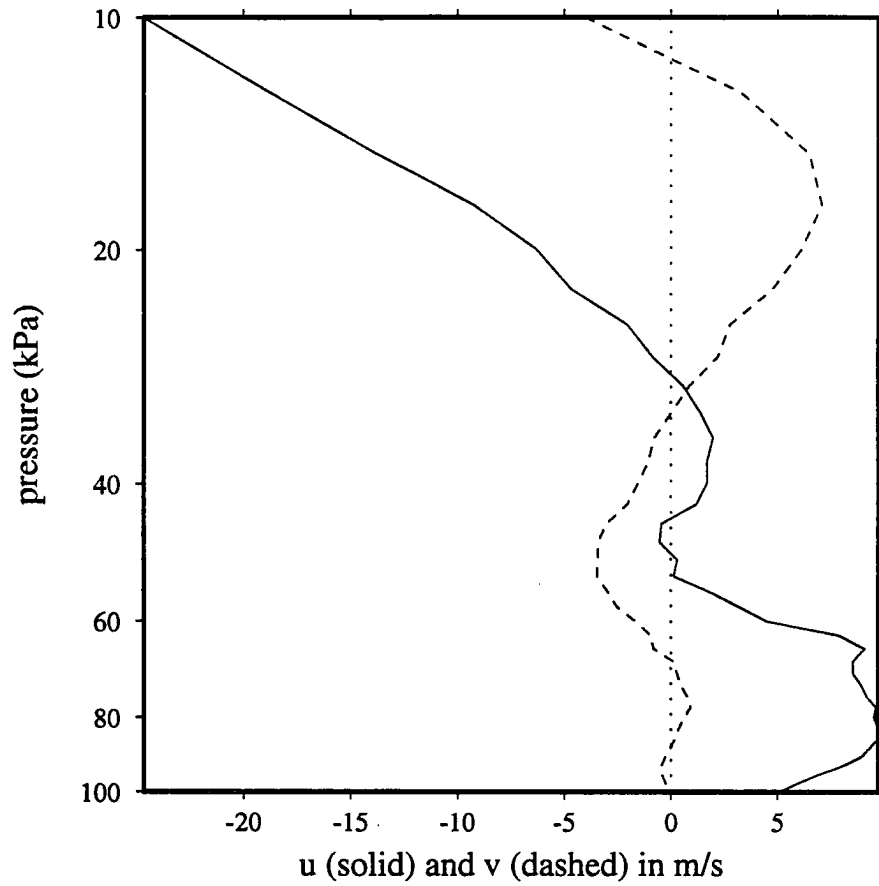
Figure 4.11: A mean wind profile for 18Z 21 December 1992 through 18Z 23 December 1992.

easterlies and southeasterlies above 30 kPa (Figure 4.11).

The most intense two-day disturbance passed over the IFA at 18Z on 24 December 1992 (Figure 4.12). It appeared as a region of high cloudiness more than 1500 km across. Its structure was similar to that of the previous case--there were numerous individual clusters embedded within the disturbed area. From 00Z 24 December through 18Z 24 December, the disturbance moved westward at around 15 m s^{-1}. After 00Z 25 December the cloudiness dispersed and then regenerated to the east of the IFA. The IFA wind profile was nearly identical to that of the previous case (Figure 4.13).

The sixth two-day disturbance hit the IFA at 12Z on 19 January 1993 (Figure 4.14). At 18Z 18 January a plume of high cloudiness lay just north of the equator from 160° to 170° E. In the following 24 hours convection developed to the west of this plume, and eventually spread towards the southwest. During this time, the area with the highest cloud tops moved at an average speed of about 11 m s^{-1}. By 18Z 19 January an arc of high cloudiness more than 1500 km long lay across the IFA. This arc gradually dispersed, moving little. The IFA winds were weak throughout the troposphere (4.15).

4.3 Composite Observations

This section contains composite surface, satellite, and sounding observations of the two-day disturbances discussed in the previous section. These observations document the nature and intensity of the disturbances' convection, show that advection cannot explain the disturbances' movement, and provide the disturbances' kinematic structure. Each composite variable is an average taken over the six cases. Observation times are relative to the time of the lowest filtered IFA brightness temperature, which was generally when the two-day disturbance's cloudiness was centered over the IFA.
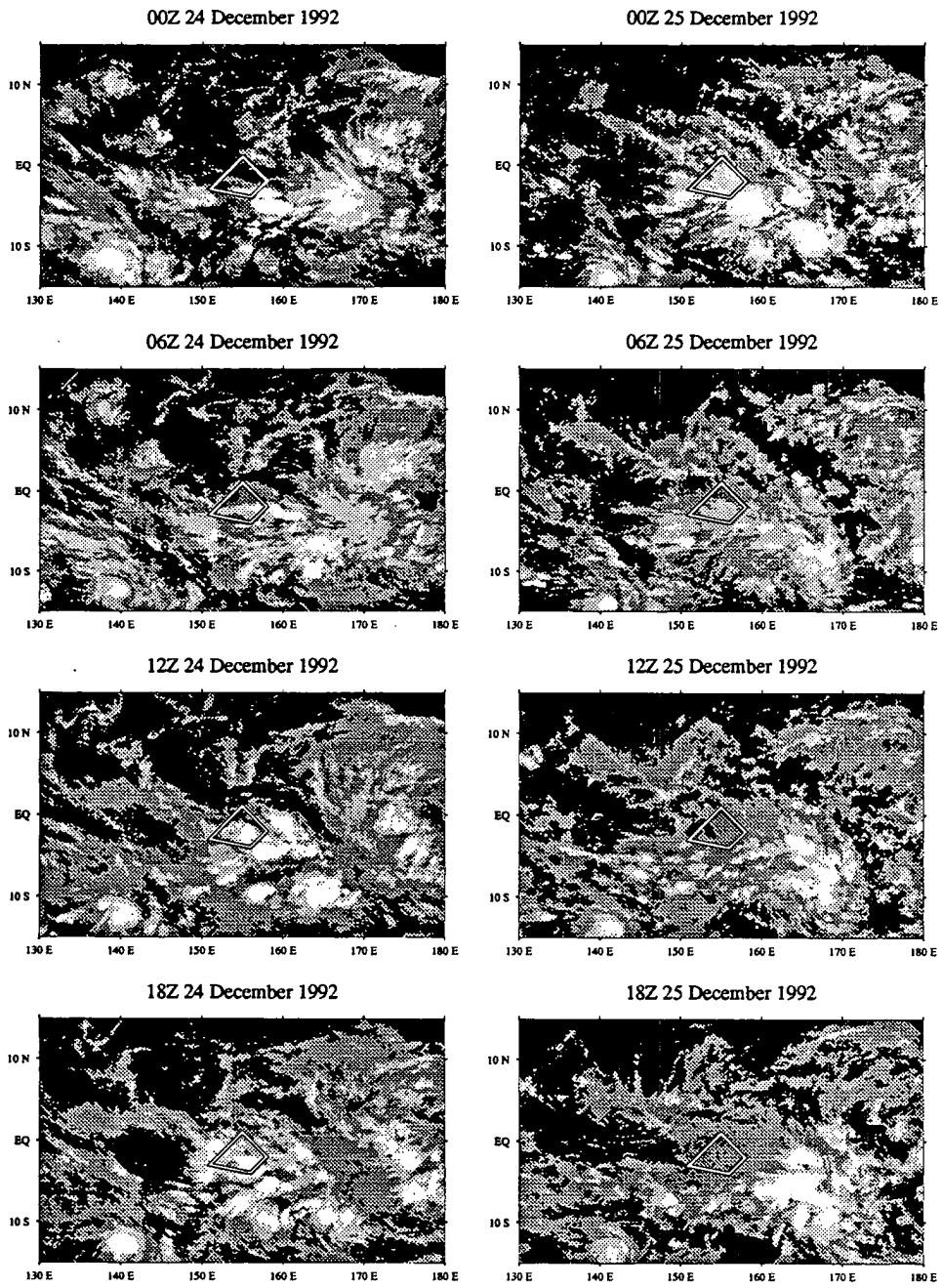
Figure 4.12: Infrared satellite view of 24 December 1992 case. The IFA is outlined.
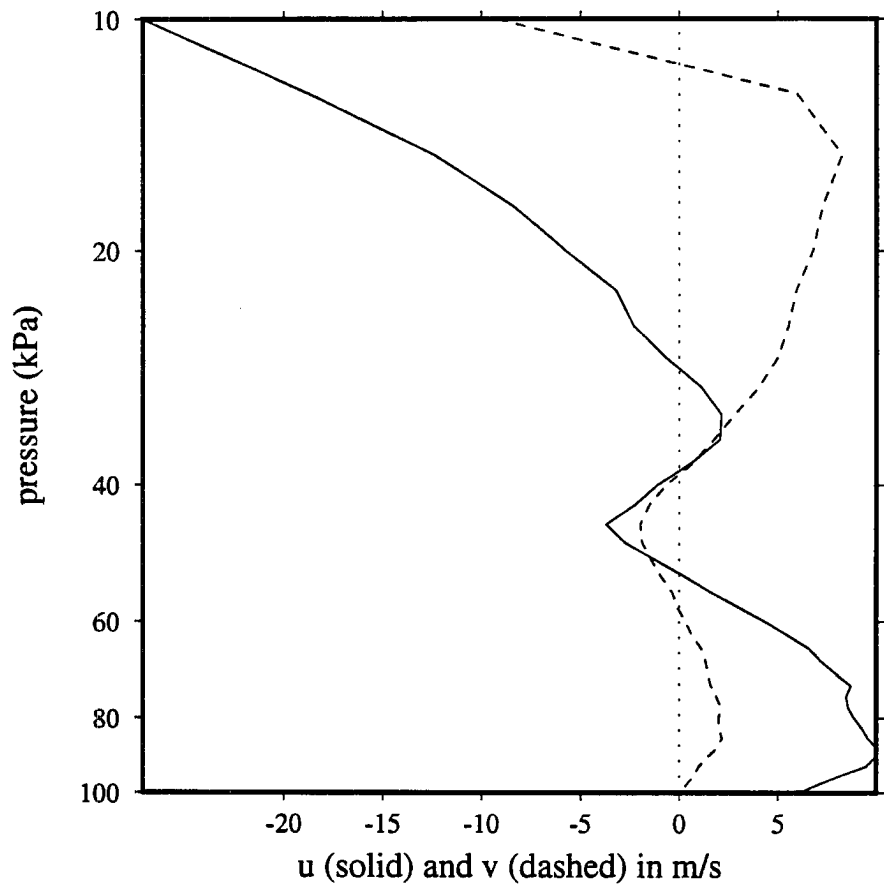
Figure 4.13: IFA mean wind profile for 18Z 23 December 1992 through 18Z 25 December 1992.
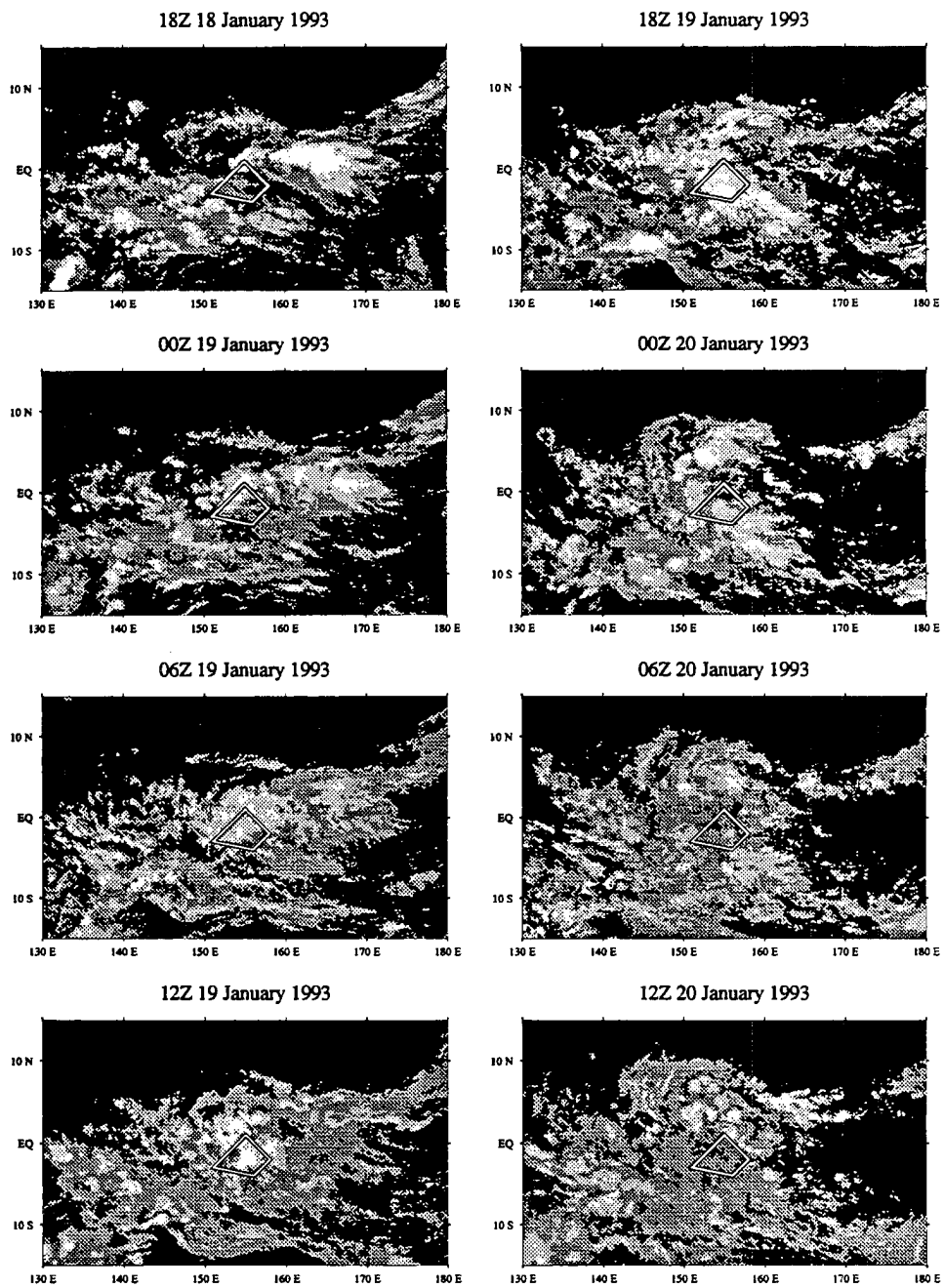
Figure 4.14: Infrared satellite view of the 19 January 1993 case. The IFA is outlined.
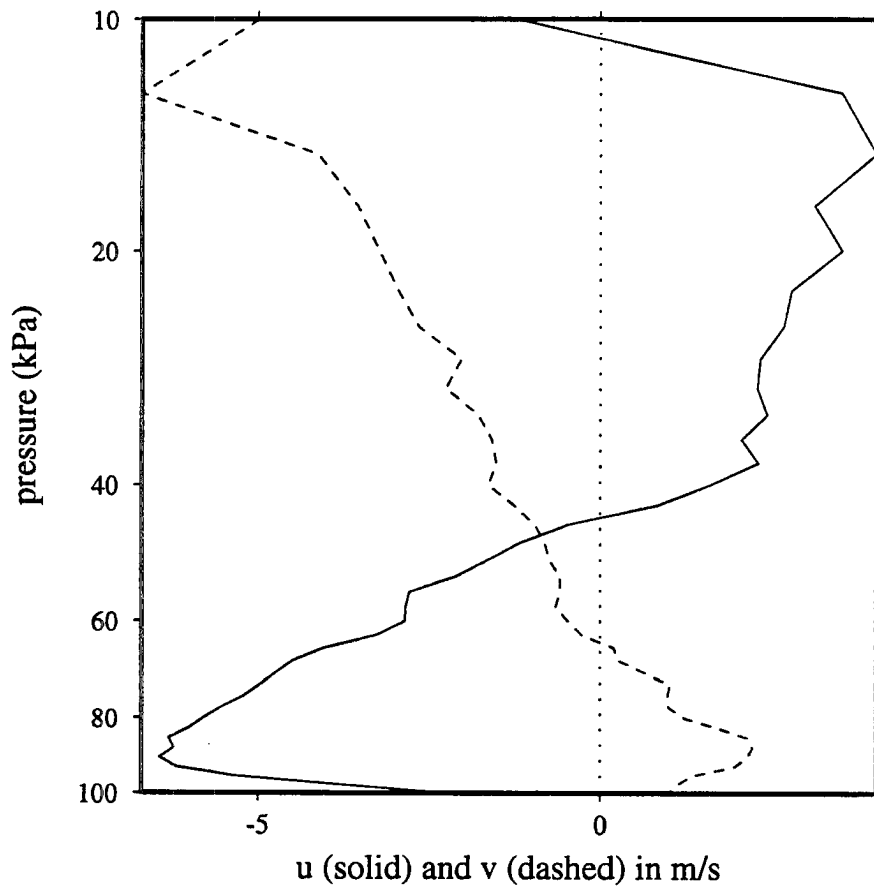
29

Figure 4.15: IFA mean wind profile for 12Z 18 January 1993 through 12Z 20 January 1993.

4.3.1 Surface Analysis

The composite two-day disturbance is responsible for substantial rainfall (Figure 4.16). From day -1 to day .75, 4.8 cm of rain accumulates over the IFA. The rain rate peaks at 1.8 mm hr^{-1} at day -.25, and the rain nearly stops by day .75. The measurements shown in Figure 4.15 are 24-hour block averages, so the duration of rain may be overestimated, and its maximum intensity may be underestimated.

The composite pressure (Figure 4.17), air temperature (Figure 4.18), and wind speed fields (Figure 4.19) all support the idea that downdrafts follow the heaviest rain. Just prior to day 0 there is a .1 kPa rise in pressure, a 2 m s^{-1} increase in wind speed, and a 2°C drop in air temperature. The cooling and drying which accompany these downdrafts are short-lived, however. Thanks to a warm sea surface (Figure 4.18) and surface wind speeds of 6-8 m s^{-1} (Figure 4.19), the temperature and dew point fields completely recover by day 1. Young et al (1995) found similar changes in temperature and wind, and a similar recovery time in their study of COARE convective wakes.

Unlike the 4-5 day disturbances observed during the COARE IOP (Numaguti et al, 1995), the two-day disturbance is not accompanied by a shift in surface wind direction (Figure 4.19). The surface wind is generally west-northwesterly at 3 m s^{-1} during disturbance passage. There is, however, a 2 m s^{-1} increase in the westerly component of the wind around day 0.

4.3.2 Satellite Analysis

An infrared satellite view of the composite two-day disturbance is shown in Figure 4.20. The disturbance originates to the east of the IFA (155 E, 2 S), strengthens as it moves westward, and diminishes after it passes the IFA. At peak intensity the disturbance has a scale of about 1000 km and a minimum brightness temperature below − 50°C. The disturbance's size and movement are similar to those of the composite two-

31
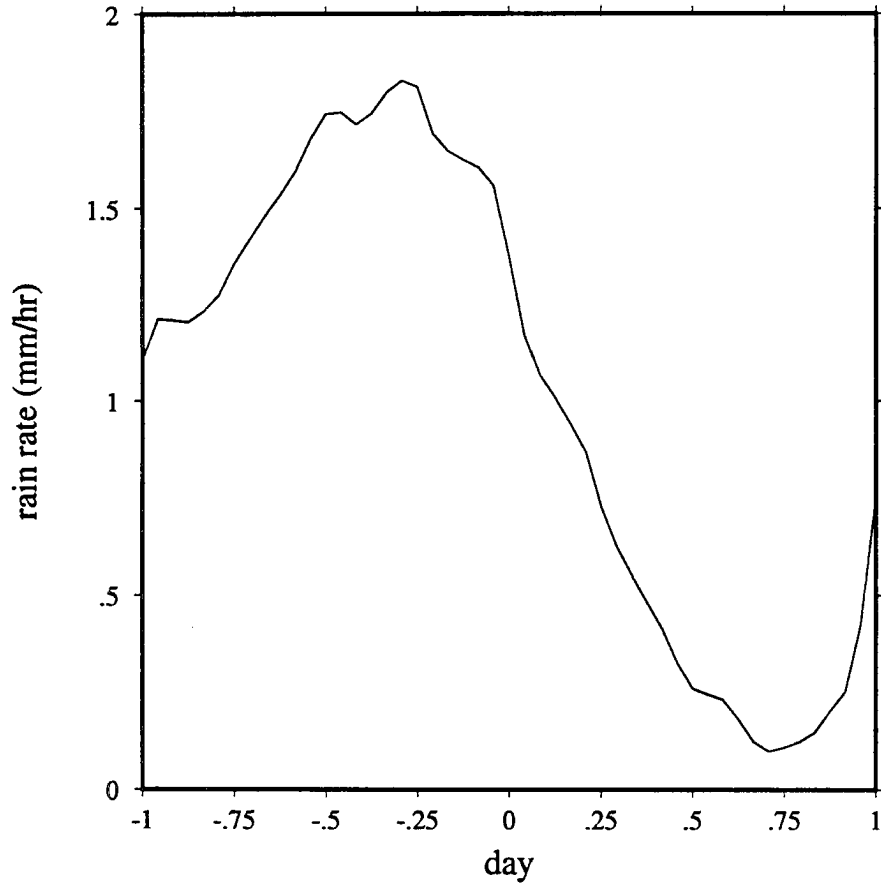
Figure 4.16: Composite IFA rain rate. The rate is a 24-hour block average of data from the WHOI and ATLAS moorings and the ships Moana Wave and Wecoma.
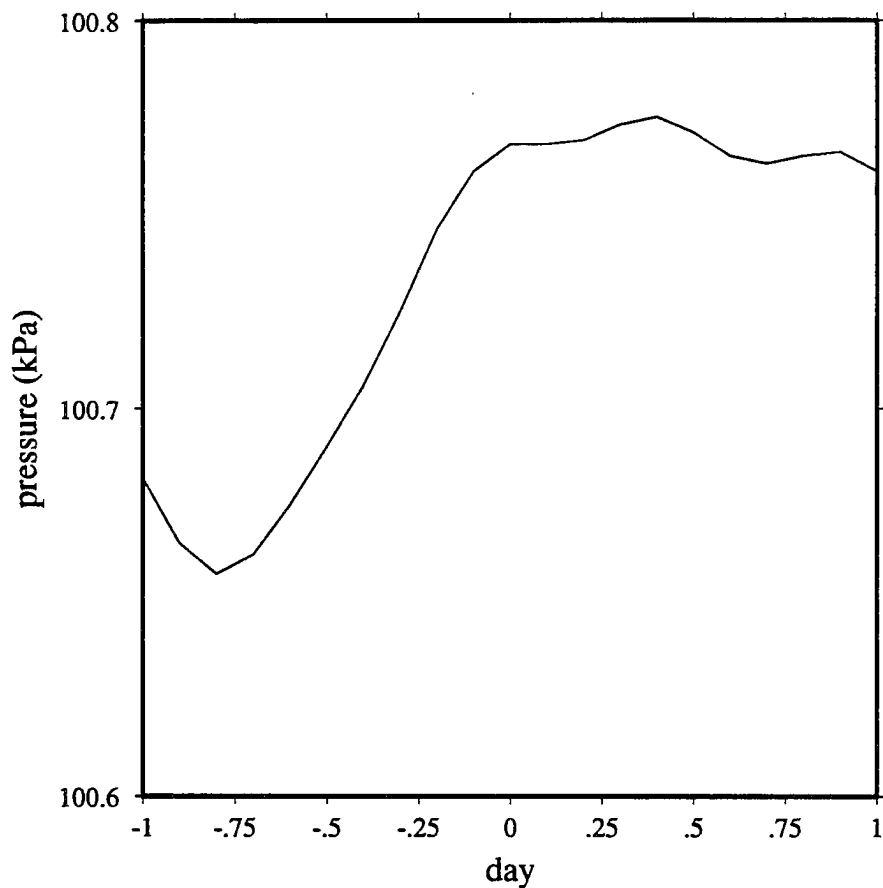
Figure 4.17: Composite IFA surface pressure. The semi diurnal variation has been fil-

tered out.

Figure 4.18: Composite IFA surface air temperature (solid), dew point (dashed), and sea surface temperature (dotted).

Figure 4.19: Composite IFA surface zonal wind (solid), meridional wind (dashed), and wind speed (dotted).

Figure 4.20: Composite infrared brightness temperature. The contour interval is 14^oC and white denotes values of less than -38^oC.
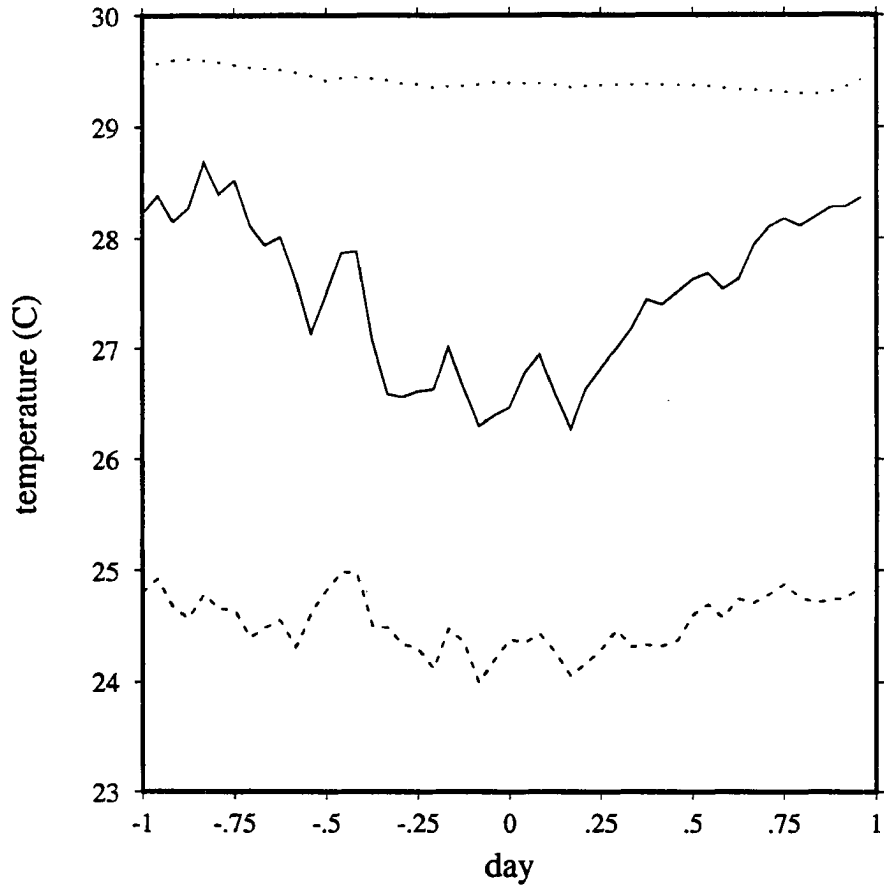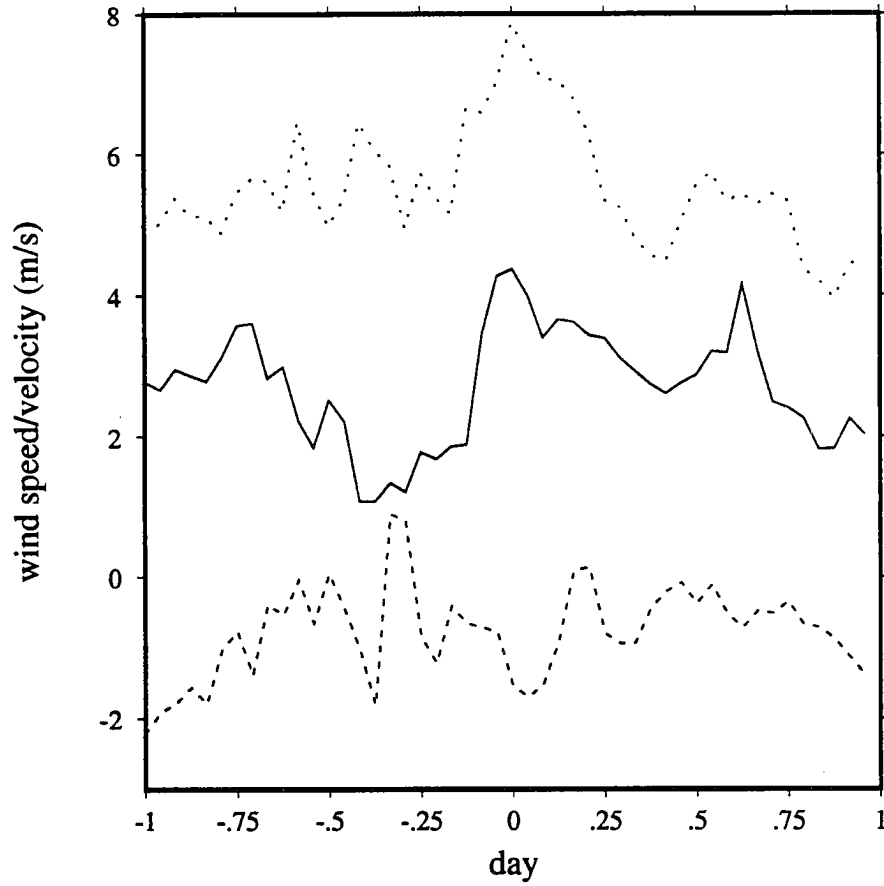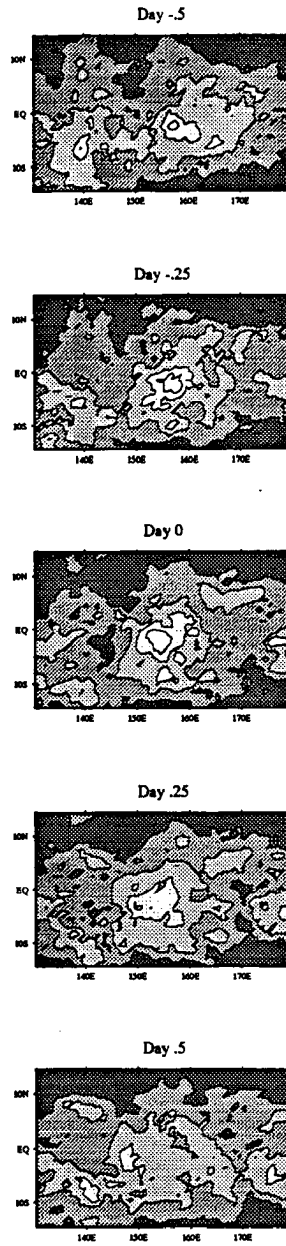
36

day disturbance constructed by Takayabu (1994).

The westward propagation of the disturbance may be quantified with the aid of a composite time-longitude series of brightness temperature (Figure 4.21). The signal of the composite disturbance lies along the diagonal of this figure's plotting domain. Hence the rate of westward propagation equals 50° longitude per 4 days or 16 m s^{-1}. Composite two-day disturbances constructed by other investigators also propagated westward at about the same speed--19 m s^{-1} in Takayabu (1994) and 15 m s^{-1} in Hendon and Liebmann (1994).

Figure 4.21 shows that the composite two-day disturbance is preceded by another two-day disturbance and trailed by yet another. All three disturbances propagate at the same rate. Each disturbance originates to the east of where its predecessor originated, so that over the 4-day period the center of convection moves slowly eastward. Nakazawa (1988, 1995), Hendon and Liebmann (1994) and others previously noted that western Pacific equatorial convection often occurs in westward-moving disturbances within eastward-moving envelopes.

4.3.3 Sounding Analysis

Time-pressure series of humidity and vertical velocity reveal the nature of the two-day disturbance's convection (Figures 4.22 and 4.23). Around day -.75 there is shallow convection, which appears as upward motion below 40 kPa. This convection is capped off by subsiding, dry air from 20 to 40 kPa. Between day -.75 and day 0 the convection deepens and intensifies, and it moistens the entire troposphere. Between day 0 and day .5 there is a transition from convective to stratiform precipitation, and subsidence and drying develop below 70 kPa. This transition is similar to the one noted by Houze (1982) in his study of tropical cloud clusters.
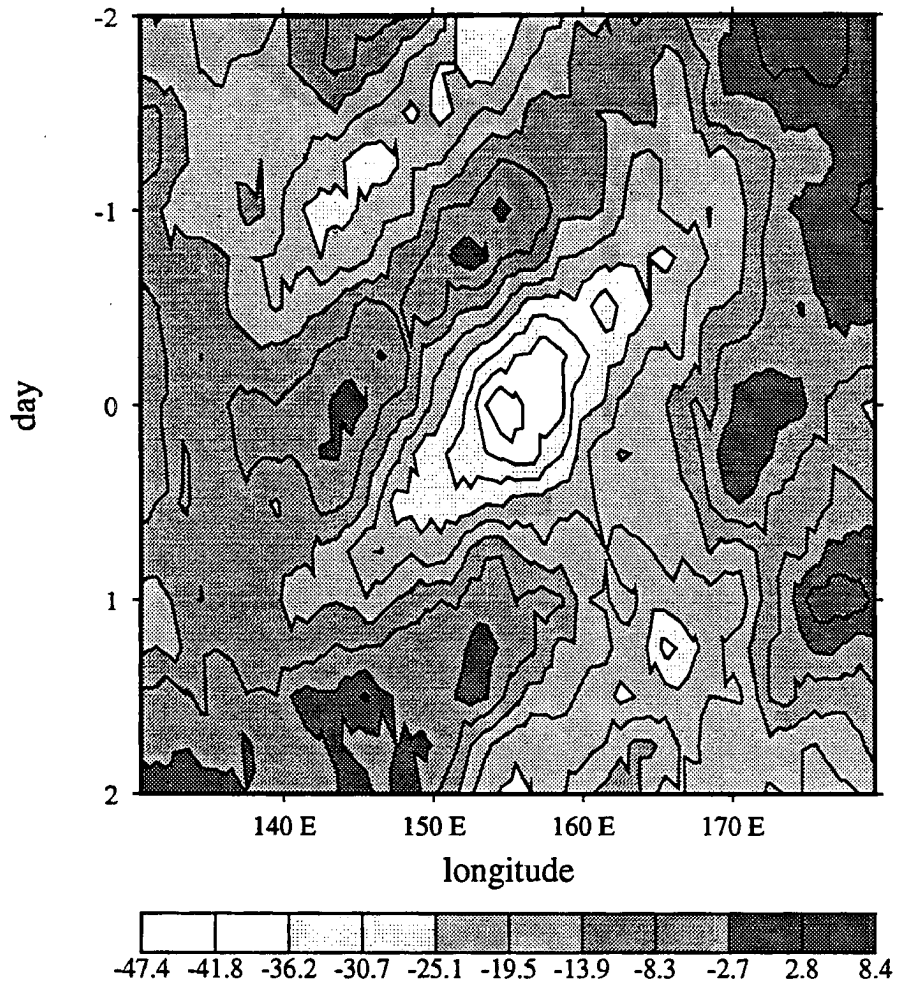
Figure 4.21: Composite time-longitude series of brightness temperature (C). Averaging is done from 5 S to 5 N for all but two cases (December 22, 24). For these cases the averaging is done from 10 S to the Equator.
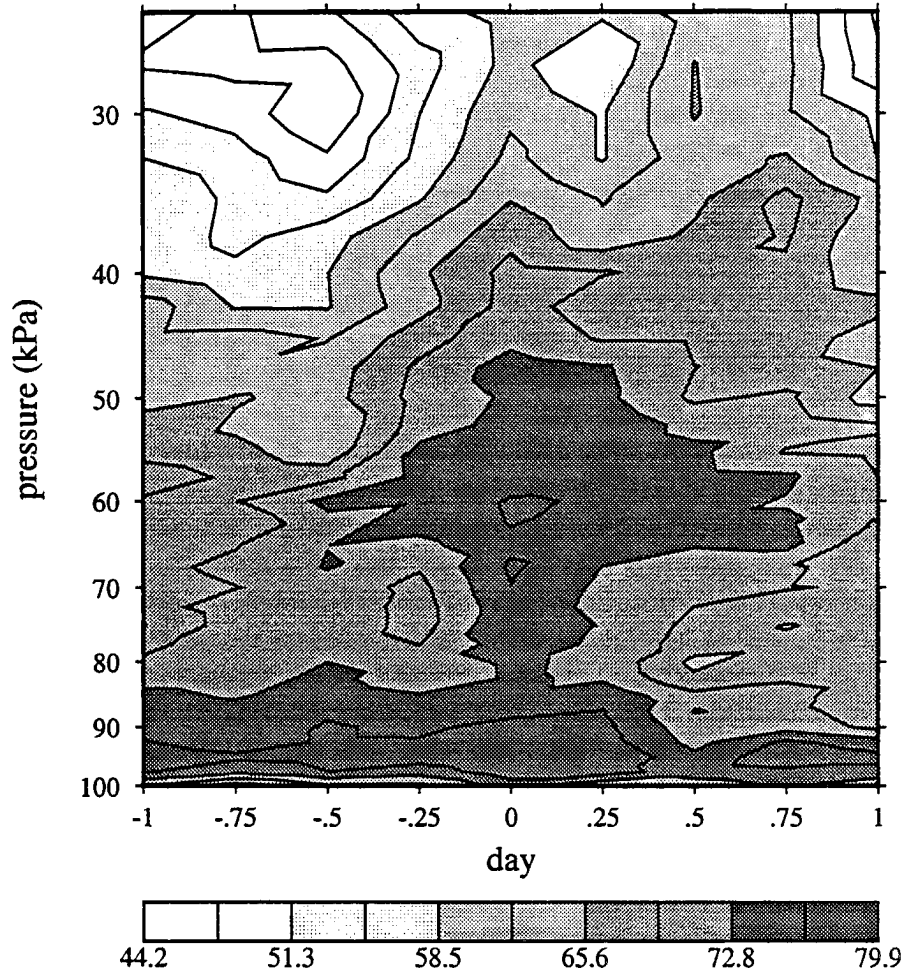
Figure 4.22: Composite time-pressure series of IFA relative humidity (%).

Figure 4.23: Composite time-pressure series of pressure velocity, $\dfrac{DP}{Dt}$ (Pa s^{-1}). The data

for this figure was generously donated by Xin Lin of Colorado State University.

40

The convection apparently diminishes on day .5 because of depleted Convective

Available Potential Energy (CAPE) (Figure 4.24). Between day -1 and day .5 CAPE falls

from 450 J kg^{-1} to 180 J kg^{-1}. Downdrafts that transport cool, dry air to the boundary

layer are responsible for this reduction of CAPE. After the convection and accompanying
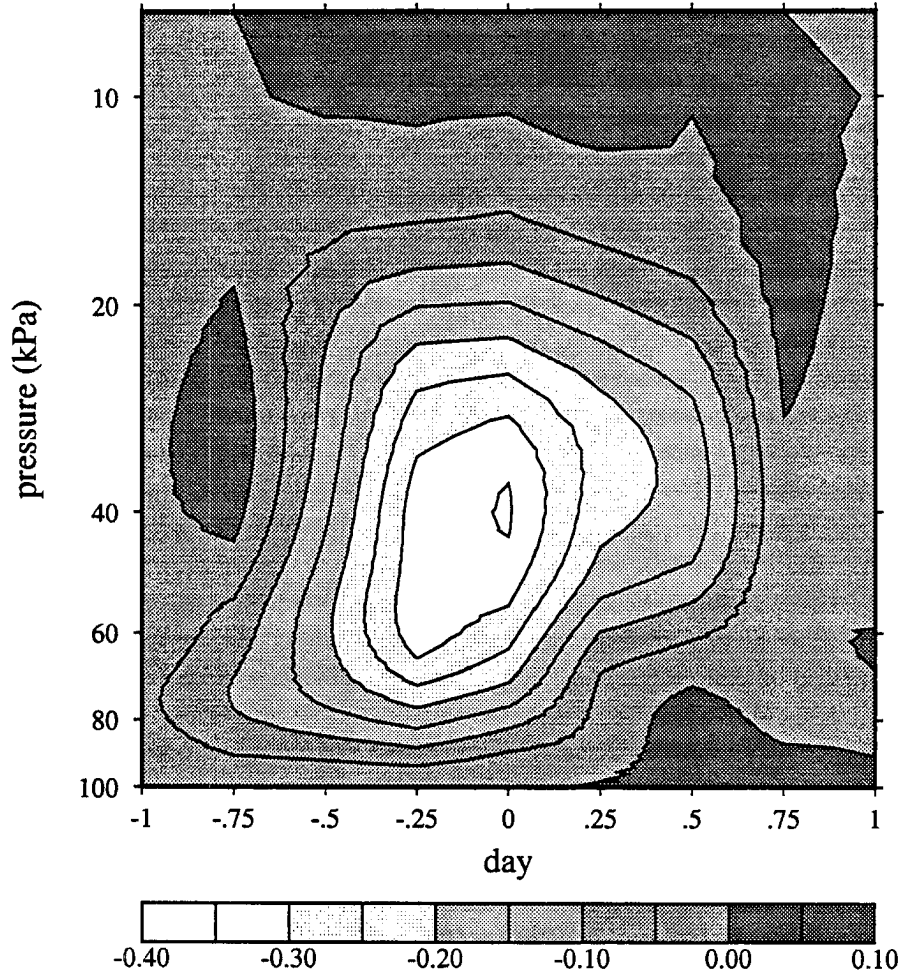
downdrafts end, CAPE recovers rapidly reaching predisturbance levels by day 1.0. This

12 hour recovery is typical of COARE convective wakes (Young et al, 1995).

Although CAPE recovers by day 1, convection remains suppressed then (Figures

4.16, 4.21, 4.23). The cause of this suppression may be the condition of the air between

70 and 90 kPa--it is warm and dry (Figures 4.22 and 4.25). The fact that this air is warm

implies high Convective Inhibition (CIN)--it is nearly twice as high on day 1 as on day -1

(Figure 4.24). The fact that this air is dry means entrainment rapidly reduces the

buoyancy of rising air parcels. Figures 4.22, 4.24 and 4.25 support Takayabu's (1994)

suggestion that the lower atmosphere takes about 2 days to recover from deep convection.

The time series of perturbation temperature (Figure 4.25) is very similar to that of

the 4-5 day waves studied by Reed and Recker (1971). In both time series the heaviest

convection is accompanied by a cooling near the tropopause, a warming from 20 to 50

kPa, and a cooling below 50 kPa which is most intense near the surface.

The sounding observations of IFA winds show that advection cannot explain the

composite disturbance's movement (Figure 4.26). When the disturbance passes over the

IFA there are weak westerlies from the surface to 65 kPa, weak northeasterlies from 65 to

20 kPa, and strong easterlies above 20 kPa. The mean flow below 20 kPa is easterly at 2

m s^{-1}, 14 m s^{-1} slower than the movement of the composite disturbance.

There may instead by a dynamical mechanism of propagation. Time series of IFA

perturbation winds (Figures 4.27 and 4.28) show that the 2-day disturbance's convection

excites two internal modes. Between day -.5 and day 1, a couplet of lower-level westerlies

and upper-level easterlies becomes a couplet of lower-level easterlies and

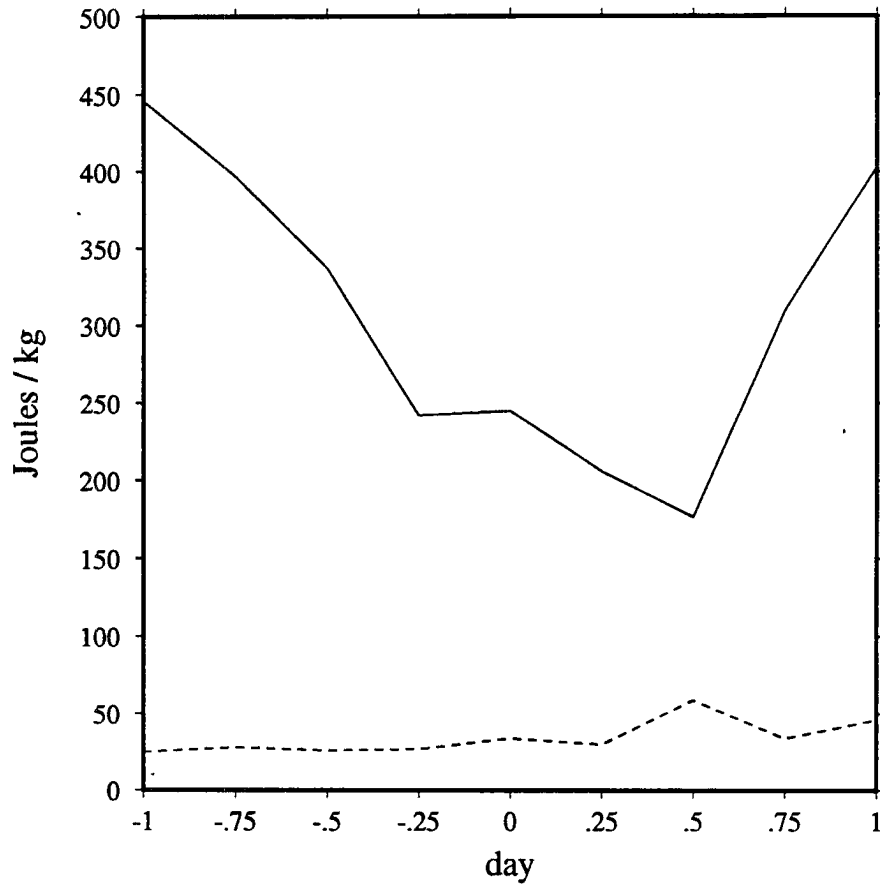Figure 4.24: Composite IFA CAPE and CIN. The method of calculating these variables is discussed in chapter 2.
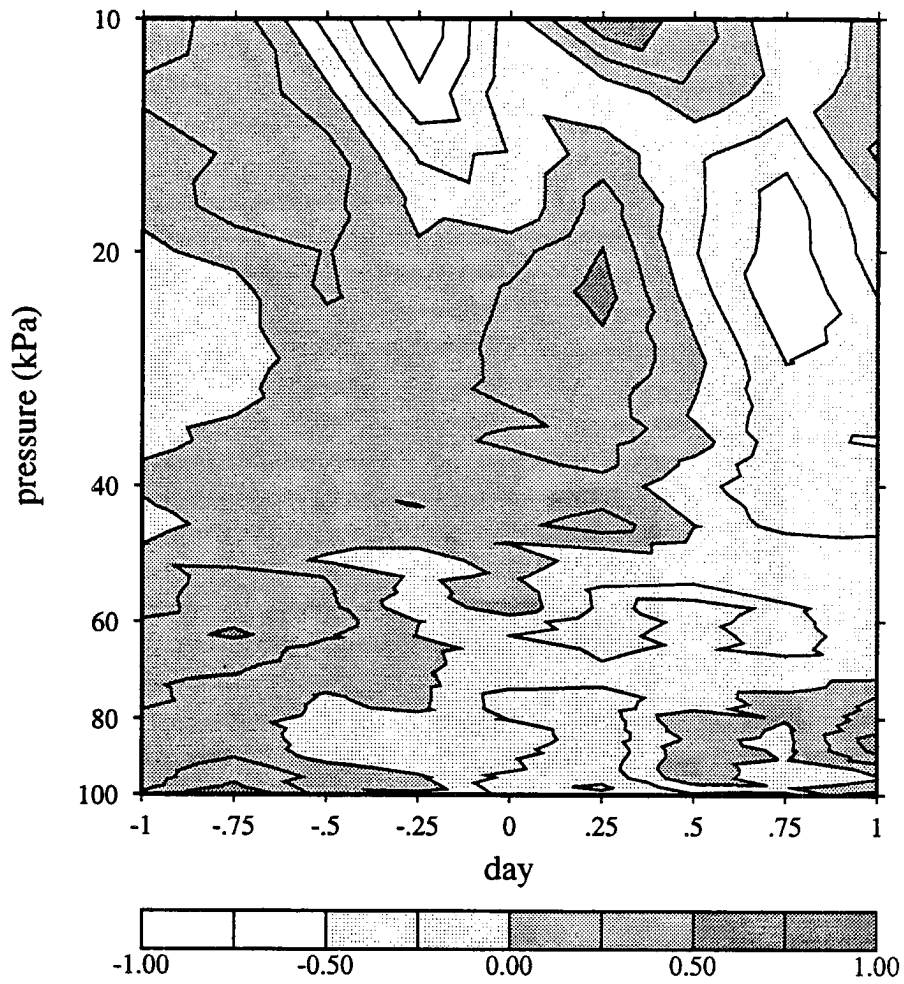
Figure 4.25: Composite time-pressure series of IFA perturbation temperature (C).
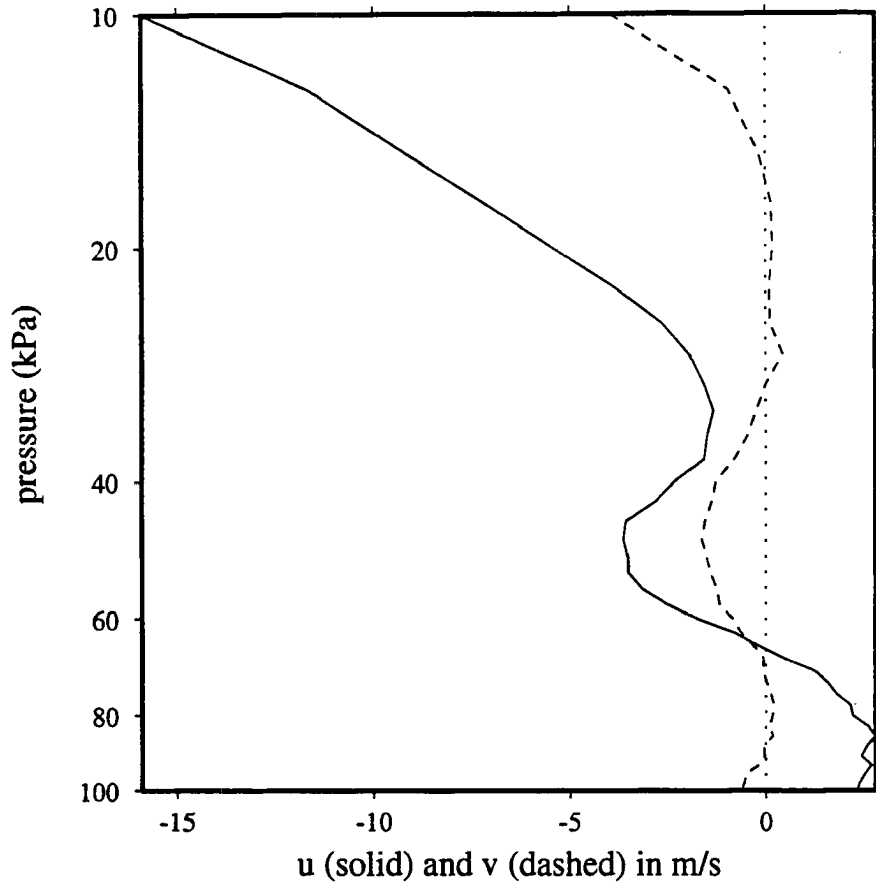
Figure 4.26: Composite IFA mean wind profile.
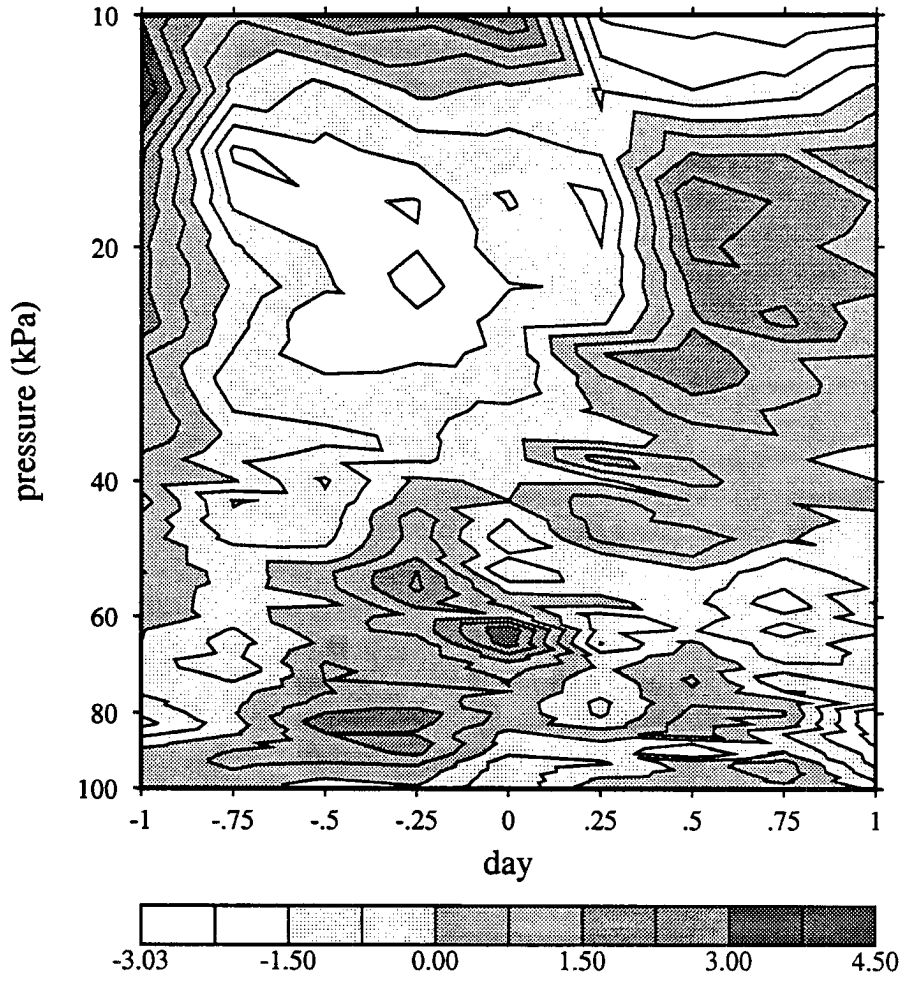
Figure 4.27: Composite time-pressure series of IFA perturbation zonal wind (m s^{-1}).
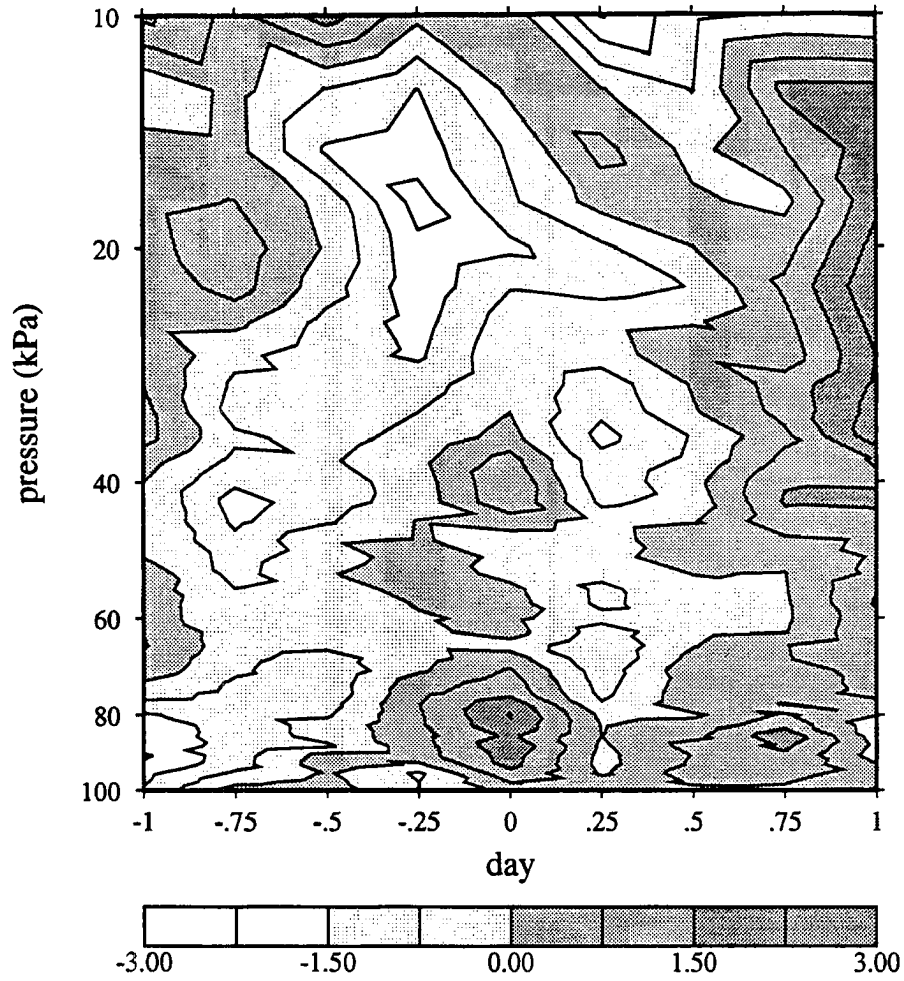
Figure 4.28: Composite time-pressure series of IFA perturbation meridional wind ($m\ s^{-1}$).

upper-level westerlies. These flow features along with the lower-level southerlies and upper-levels northerlies around day 0 (Figure 4.28) are evidence that the first internal mode has been excited. Between day 0 and day .75 a couplet of lower-level easterlies and westerlies at 60 kPa becomes a couplet of lower-level westerlies and easterlies at 60 kPa, supporting the idea that a second internal mode has been excited. Chapter 5 further discusses these two modes and their role in the propagation of the disturbance.

Chapter 5

MODELING THE TWO-DAY DISTURBANCE

Numerical simulations of the two-day disturbance's convective heating explain the disturbance's propagation. The heating excites two internal modes which combine to favor new convection to the west of the heat source. One of these modes propagates at 17 m s^{-1}, the approximate speed of the composite disturbance constructed in Chapter 4.

5.1 Simulation Neglecting the Coriolis Force

For the first simulation the Coriolis force is neglected. This is done in order to evaluate the importance of the β-effect, which is included in the second simulation.

After three hours of heating, the perturbation temperature field (Figure 5.1) resembles the heat source. Low-level winds converge towards the geopotential minimum at the heating center (Figures 5.2 and 5.3), and upper-level winds diverge from a geopotential maximum there (Figures 5.2 and 5.4).

After six hours of heating there is evidence of dispersing internal modes (Figure 5.1). For a discussion of the theory of these modes the reader is referred to Fulton and Schubert (1985), Nicholls et al (1991), Pandya et al (1993) and Mapes (1993). The first mode, which propagates at about 50 m s^{-1}, has warmed much of the troposphere within 1500 km of the heating center by time 6 hours (Figure 5.1). The effects of modes with shorter vertical wavelengths remain nearer to the heating center. One such mode, hereafter the second internal mode, is associated with a cooling from 10 to 19 kPa, a warming from 19 to 70 kPa, and a cooling from 70 to 100 kPa (Figure 5.1). Mapes and Houze (1995) show a similar temperature field after 6 hours of heating in their simulations of IFA convection.

48

Figure 5.1: Vertical cross-section of perturbation temperature (C) along the equator for the model simulation neglecting the Coriolis force.
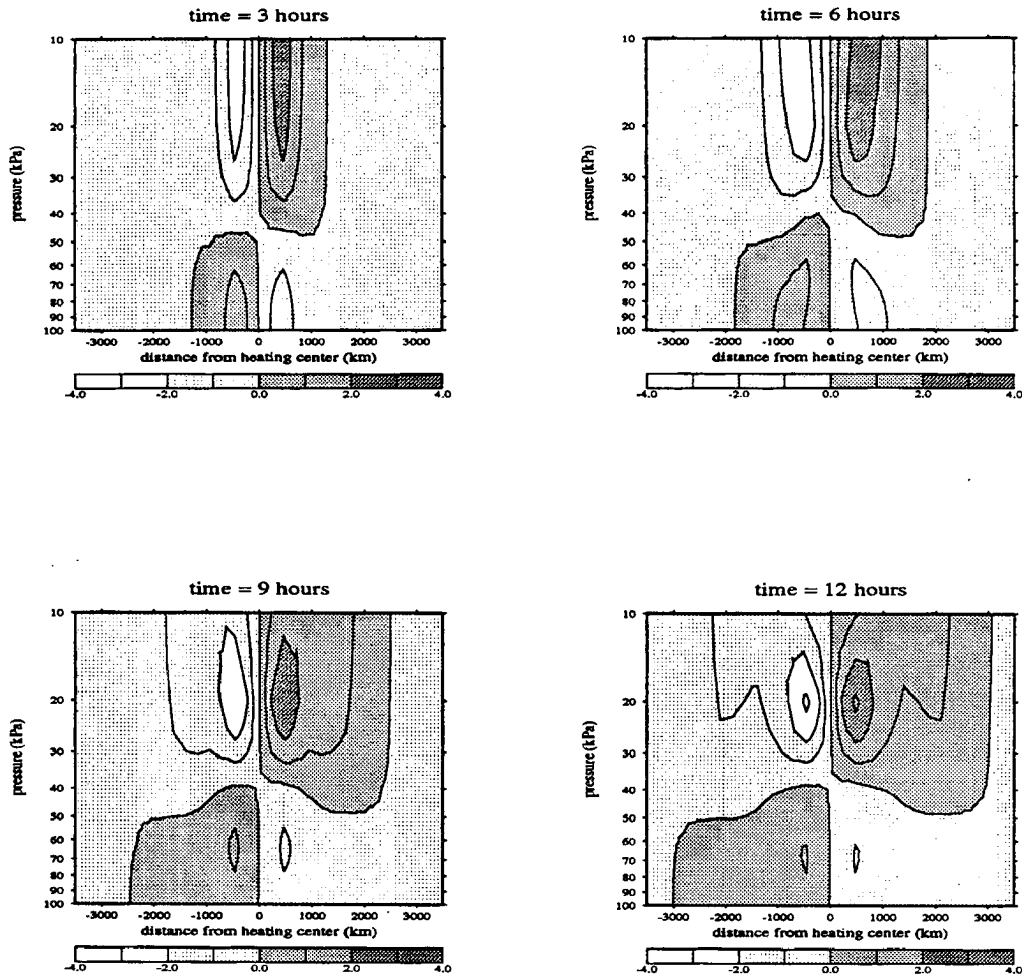
Figure 5.2: Vertical cross-section of perturbation zonal wind (m s^{-1}) along the equator for the model simulation neglecting the Coriolis force.
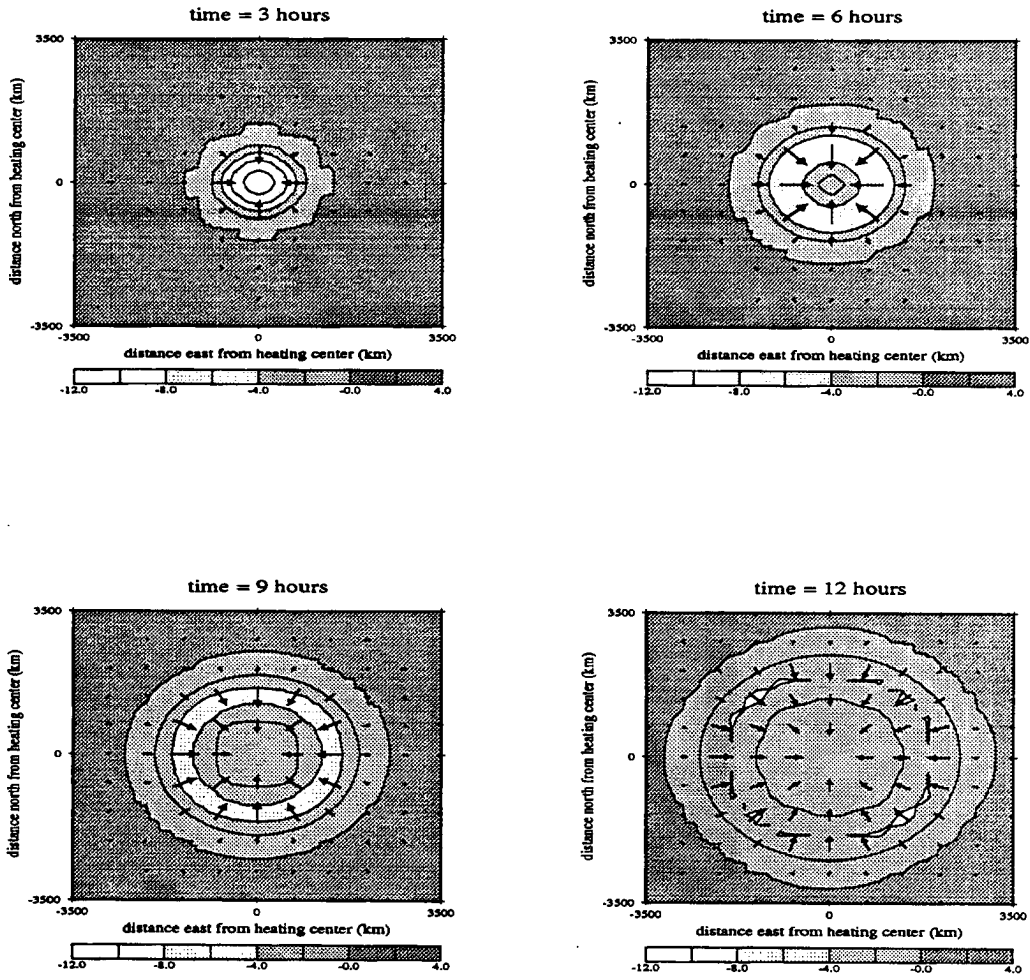
Figure 5.3: Horizontal cross-section of perturbation height (m) and wind vectors at 100 kPa for the model simulation neglecting the Coriolis force.
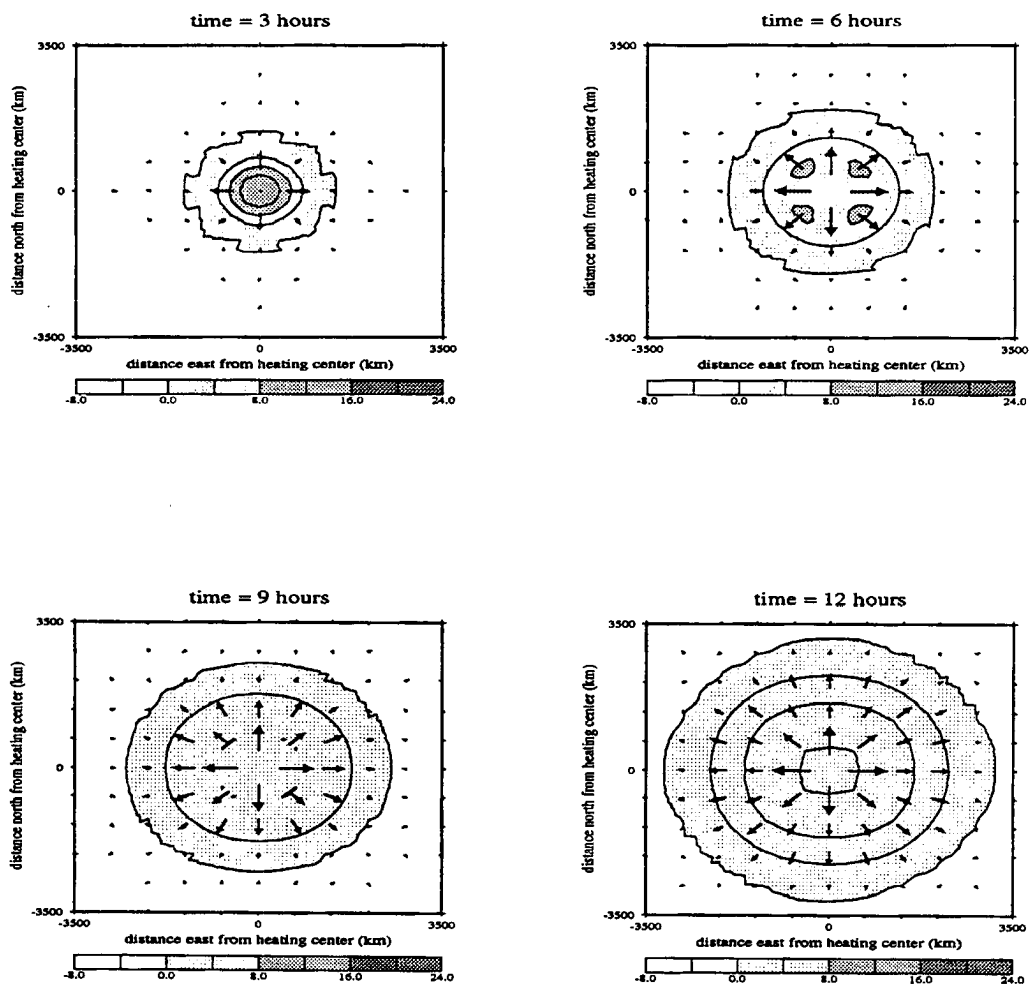
Figure 5.4: Horizontal cross-section of perturbation height (m) and wind vectors at 20 kPa for the model simulation neglecting the Coriolis force.

Between time 6 hours and time 12 hours the modes continue to disperse. By time 12 hours the warming on the leading edge of the first internal mode has reached more than 2000 km away from the heating center (Figure 5.1). Meanwhile, the lower-level cooling has spread 1000 km away from the heating center. The lower-level convergence near the heating center has become elevated by this time (Figure 5.2). Notice that, except for minor computational noise, the solution remains symmetric about the center of heating (Figures 5.1-5.4).

The primary goal of this chapter is to understand how dynamics couples with convection. To address the question of where new convection is favored I define vertical displacement as follows:

$$vertical\ displacement = \int_0^t \omega\ dt \qquad (5.1)$$

where t is time and ω denotes pressure velocity. Regions where vertical displacement is negative (where the atmosphere has been lifted) favor convection because such regions are cooler and more moist than regions that have subsided. I will not consider the vertical displacement within the heat source because this region contains both rising and sinking air (updrafts and downdrafts).

At time 3 hours much of the atmosphere adjacent to the heat source has subsided up to 0.5 kPa (Figure 5.5). The first internal mode is responsible for this subsidence and hence the subsidence spreads at 50 m s^{-1}. By time 12 hours the effects of the second internal mode are apparent--much of the lower troposphere within 1000 km of the heat source has been lifted. Mapes (1993, 1995) suggested that the lifting associated with the second internal mode may trigger new convection, and may explain the 'gregarious' nature of tropical convection.
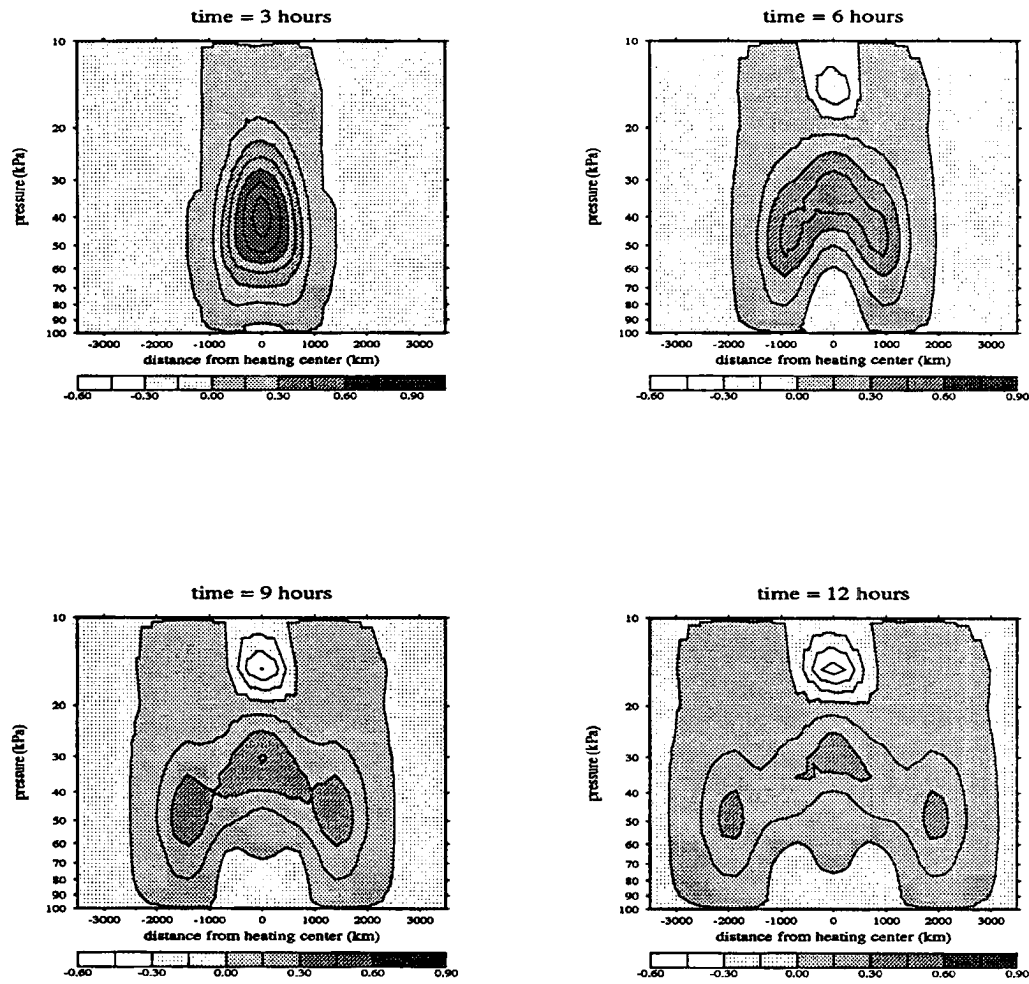
Figure 5.5: Vertical cross-section of vertical displacement (kPa) along the equator for the model simulation neglecting the Coriolis force.
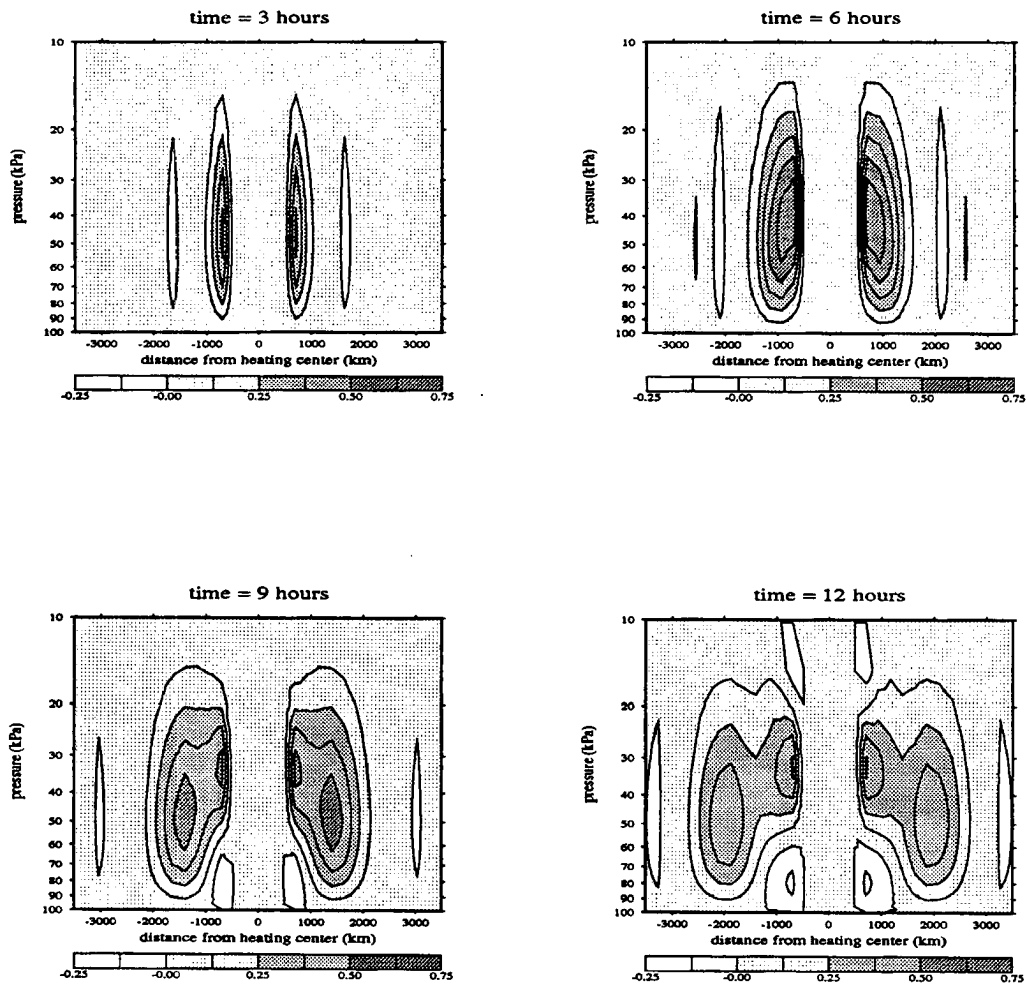
6.2 Simulation on the β-plane

The simulation on the β-plane begins to differ from the first simulation around time 6 hours. At this time the atmosphere is warmer to the east of the heating center than to its west (Figure 5.6). The latitudinal variation of the Coriolis force (hereafter β-effect) acts on the wind field associated with the first internal mode to cause this east-west asymmetry. To the west of the heat source there are lower-level westerlies (Figure 5.7) which, thanks to the β-effect, veer towards the equator leading to increased lower-level meridional convergence (Compare Figure 5.8 to Figure 5.3). To the west of the heat source there are also upper-level easterlies (Figure 5.7) which, thanks to the β-effect, veer away from the equator leading to increased upper-level meridional divergence (Compare Figure 5.9 to Figure 5.4). The combination of increased lower-level convergence and upper-level divergence leads to upward motion and adiabatic cooling to the west of the heat source. In a similar way the β-effect enhances subsidence to the east of the heat source.

By time 15 hours, the region 1000 km west of the heating center favors new convection the most (Figure 5.10). By this time the second internal mode has lifted the lower atmosphere both 1000 km to the east and 1000 km to the west of the heating center, but thanks to the β-effect, the first internal mode has sunk the troposphere more to the east of the heat source (compare Figure 5.10 to Figure 5.5). If new convection were to form in this 'most favorable' region, it would further excite the first and second internal modes favoring more convection to its west. Hence, the two-day disturbance may be caused by a coupling between convection and the first and second internal modes. The rate of westward-propagation may be related to the speed of the second internal mode (17 m s^{-1}).
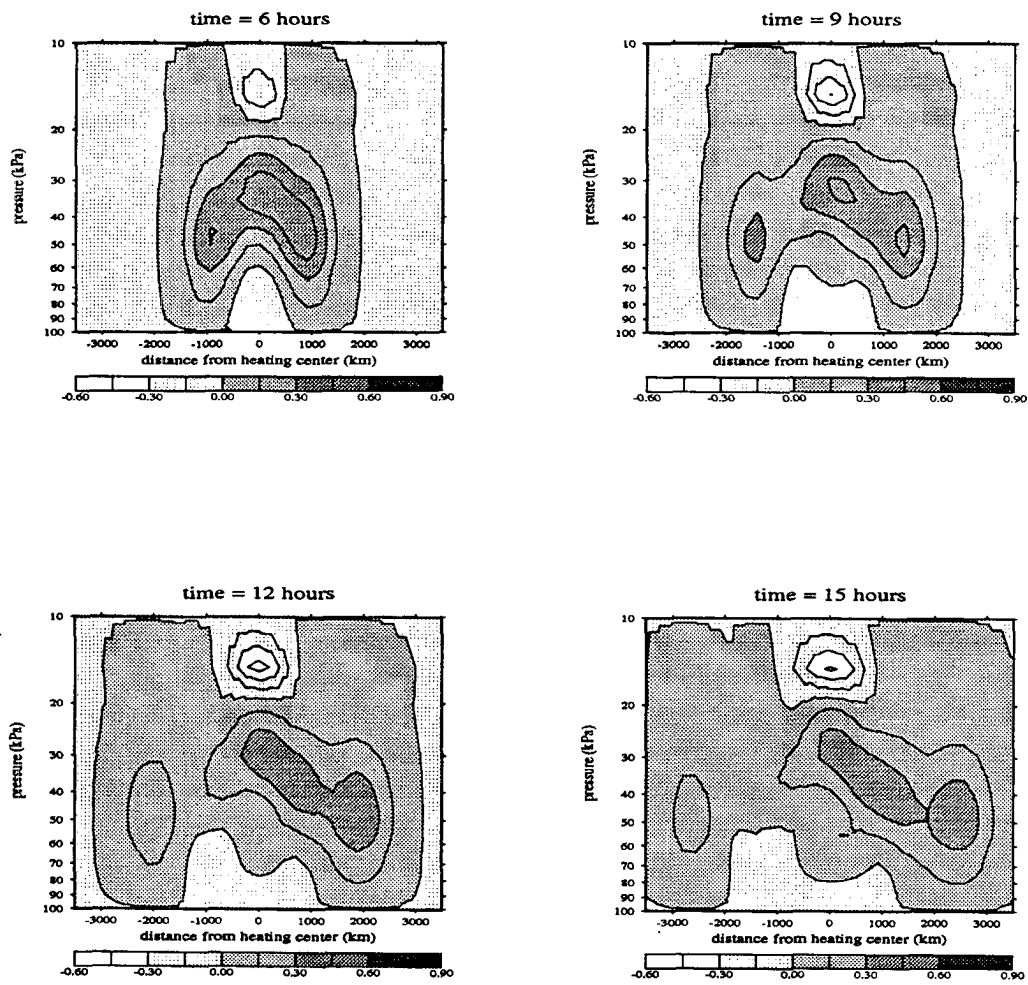
Figure 5.6: Vertical cross-section of perturbation temperature (C) along the equator for the model simulation on the β-plane.
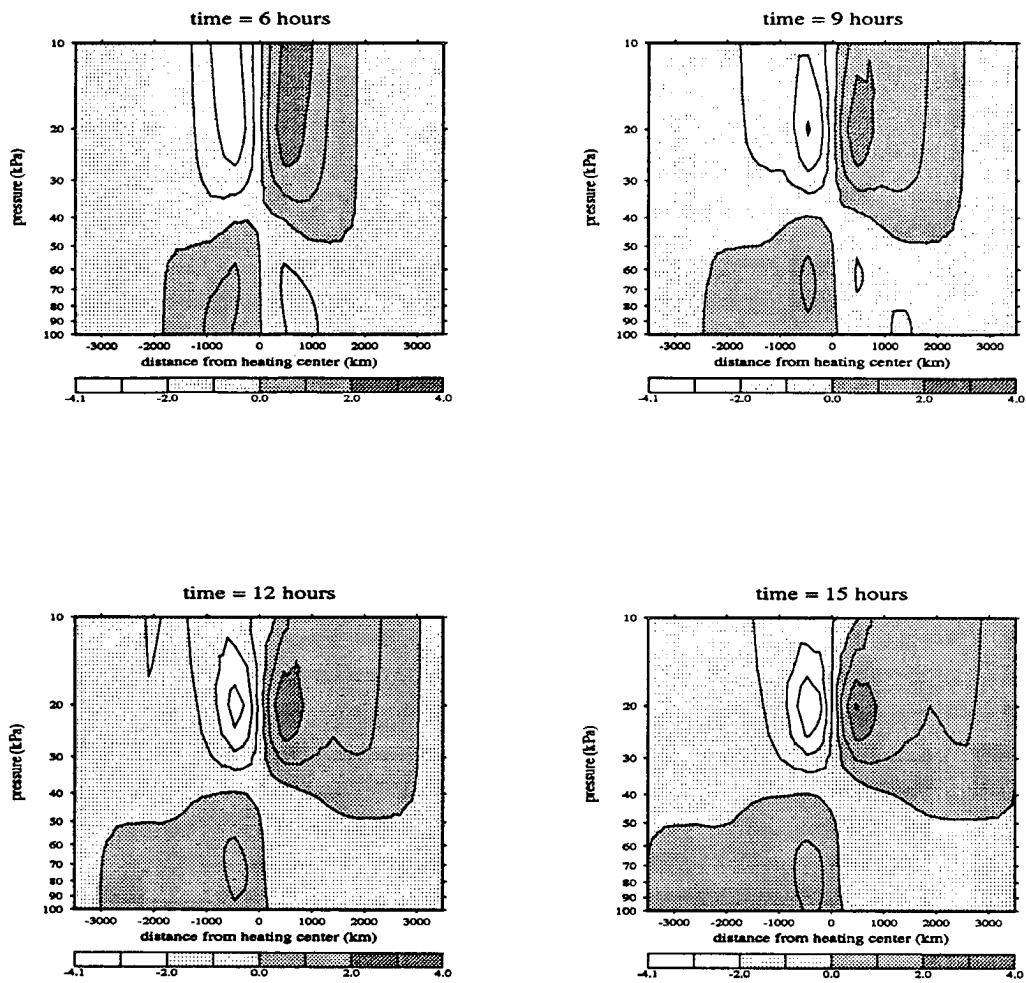
Figure 5.7: Vertical cross-section of perturbation zonal wind (m s^{-1}) along the equator for the model simulation on the β-plane.

Figure 5.8: Horizontal cross-section of perturbation height (m) and wind vectors at 100 kPa for the model simulation on the β-plane.

Figure 5.9: Horizontal cross-section of perturbation height (m) and wind vectors at 20 kPa for the model simulation on the β-plane.

Figure 5.10: Vertical cross-section of vertical displacement (kPa) along the equator for the model simulation on the β-plane.

Chapter 6

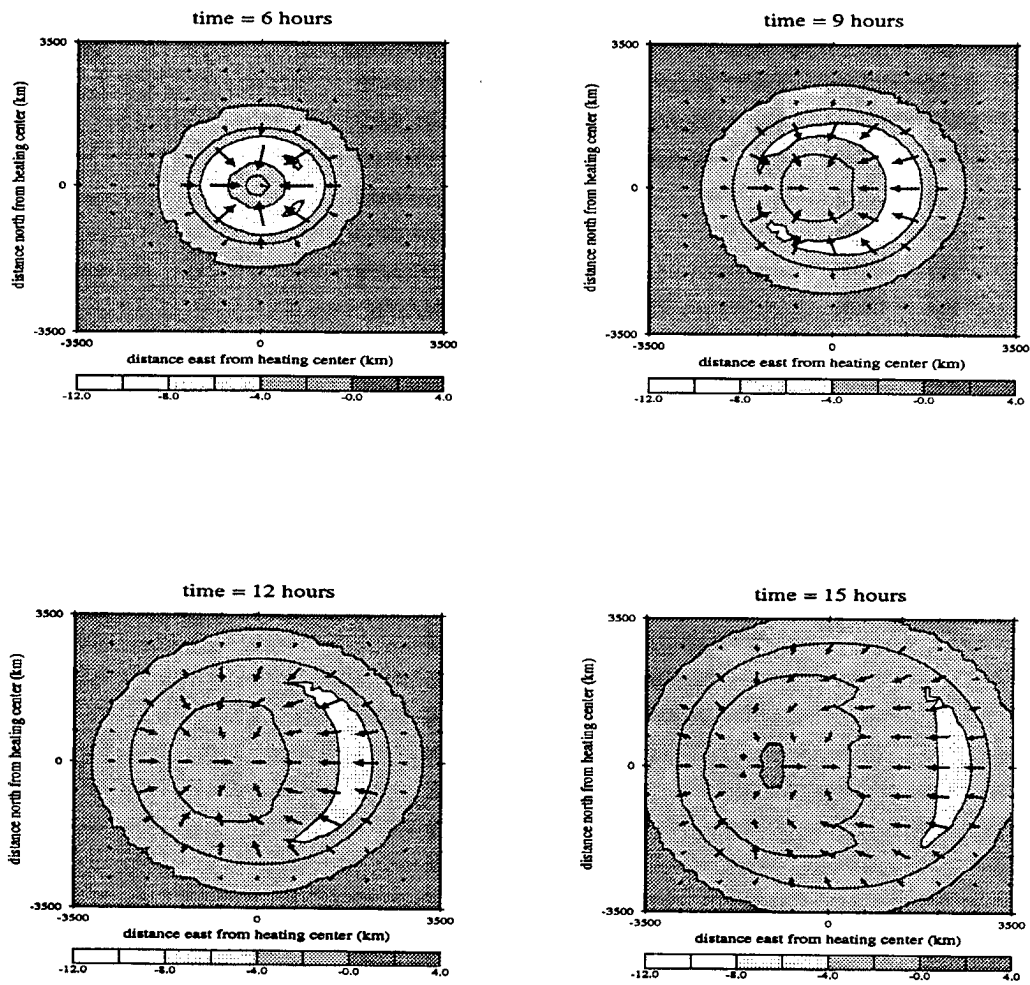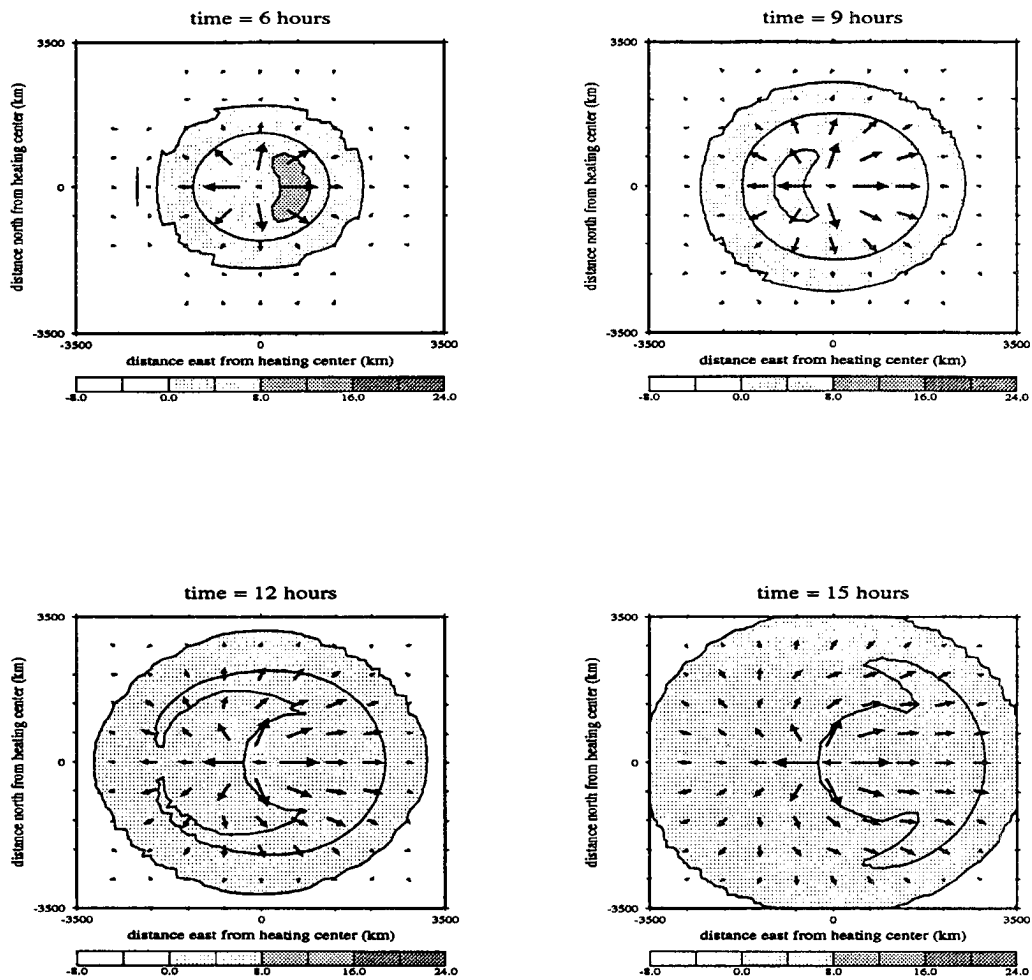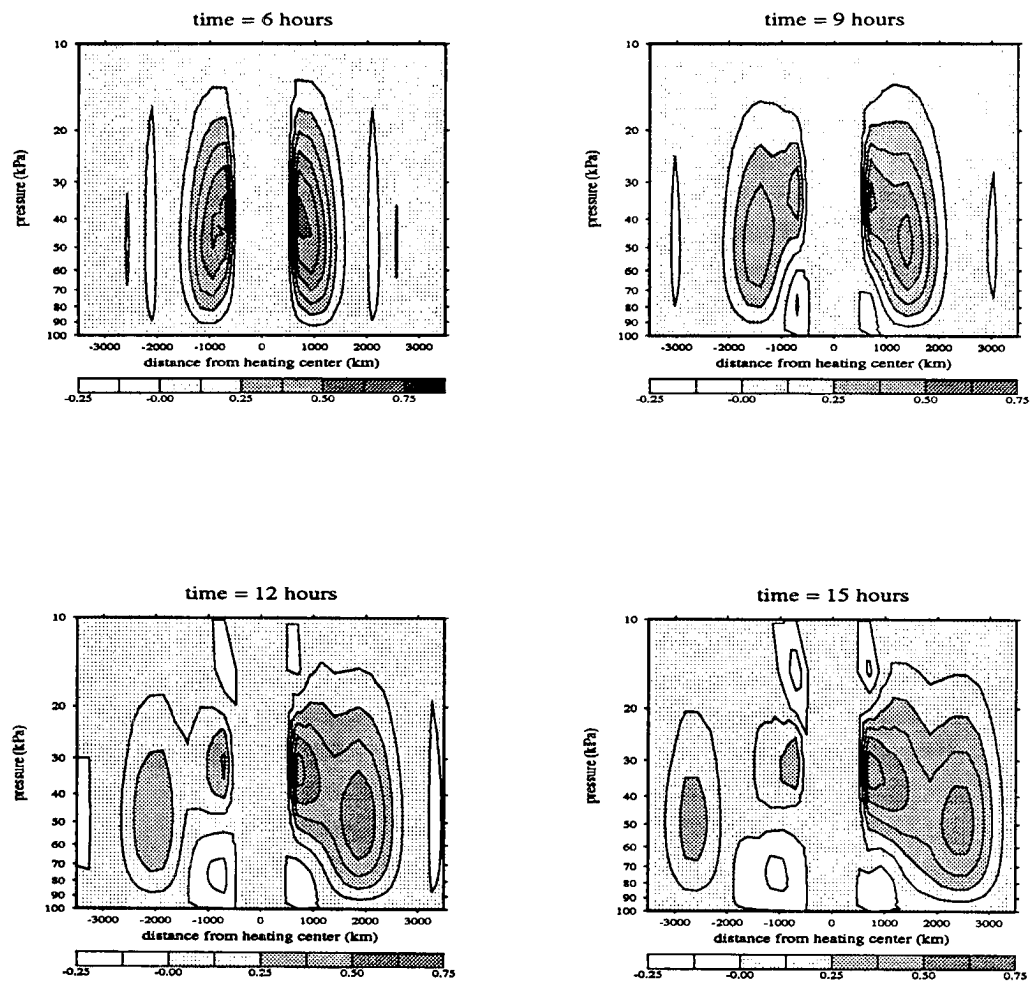# SUMMARY

Within this paper I have presented observations of the 2-day disturbances that occurred in the tropical Western Pacific during the boreal winter of 1992-1993, and I have provided a theory of how these disturbances propagated.

The satellite observations corroborated the results of other investigators (Chen, 1995; Hendon and Liebmann, 1994; Takayabu, 1994; Nakazawa, 1995). The typical COARE 2-day disturbance was an envelope of cloud clusters, and it moved westward along the equator at 16 m s^{-1}. Most of the COARE 2-day disturbances occurred within the active phase of the ISO.

The sounding and surface observations documented the convective and kinematic structure of COARE two-day disturbances. Their convection cycled through three morphologies--shallow, deep, and stratiform. It ended when Convective Available Potential Energy (CAPE) was depleted and remained suppressed when CAPE had recovered thanks to high Convective Inhibition and a dry lower troposphere. These observations support the idea that the disturbances' 2-day period is related to the recovery time of the atmosphere below the trade inversion (Takayabu, 1994). The disturbances propagated westward at about 14 m s^{-1} faster than the mean tropospheric flow, apparently through a dynamical mechanism. Time series of zonal and meridional wind showed that the disturbances' convection excited two internal modes.

Numerical simulations explain the disturbances' westward propagation. A heat source with an empirical vertical profile excites two internal modes which combine to favor new convection to the west of the heat source. The β-effect acts on the wind-field associated with the first internal mode to create a perturbation lifting through the troposphere to the west of the heat source. A second internal mode, which propagates at

17 m s^{-1}, causes lower-level lifting to spread radially from the heat source. To the west of the heat source, where these two lifting mechanisms combine, is the region that favors new convection the most. The COARE 2-day disturbances apparently propagated at 16 m s^{-1} because they moved with the second internal mode.

Although this paper has furthered the understanding of the two-day disturbance's structure and propagation, additional observational and modeling research are needed. The sounding observations presented here come from only six cases, each of which occurred in a four-month period. Creating composite time series from many years of data would yield results that were less likely to be polluted by random measurement error and exceptional cases and seasons. Simulating two-day disturbances with a model that includes a moving heat source, wind shear, and/or a convective scheme would further test theory that the disturbance is a coupling between the first and second internal modes and convection.

REFERENCES

Chen, Shuyi S., Robert A. Houze. Jr., and Brian E. Mapes, 1995: Multiscale variability of deep convection in relation to large-scale circulation in TOGA COARE. *J. Atmos. Sci.,* (in press).

Colby, Frank P. Jr., 1984: Convective Inhibition as a predictor of convection during AVE-SESAME II. *Mon. Wea. Rev.,* **112,** 2239-2252.

Fulton, Scott R. and Wayne H. Schubert, 1985: Vertical Normal Mode Transforms: Theory and Application. *Mon. Wea. Rev.,* **113,** 647-658.

Hendon, H. and B. Liebmann, 1994: Organization convection within the Madden-Julian oscillation. *J. Geophy. Res.,* **99,** 8073-8083.

Houze, R. A., Jr., 1982: Cloud clusters and large-scale vertical motions in the tropics. *J. Meteor. Soc. Japan,* **60** (special issue), 396-409.

Lau, K. M., L. Peng, C. H. Sui and T. Nakazawa, 1989: Dynamics of super cloud clusters, westerly wind bursts, 30-60 day oscillations and ENSO: a unified view. *J. Meteor. Soc. Japan,* **67,** 205-219.

Lin, Xin and Richard H. Johnson, 1995: Kinematic and thermodynamic characteristics of the flow over the western Pacific warm pool during TOGA COARE. *J. Atmos. Sci.,* (in press).

Madden Roland A. and Paul R. Julian: Observations of the 40-50 day tropical oscillation--a review. *Mon. Wea. Rev.,* **122,** 814-837.

Mapes, Brian E.: Gregarious tropical convection, 1993. *J. Atmos. Sci.,* **50,** 2026-2037.

Mapes, B. E. and R. A. Houze, Jr., 1995: Diabatic divergence profiles in western Pacific mesoscale convective systems. *J. Atmos. Sci.,* **52,** 1807-1828.

Matsuno, T., 1966: Quasi-geostrophic motions in the equatorial area. *J. Meteor. Soc. Japan*, **44**, 25-42.

Moncrieff, M. W. and M. J. Miller, 1976: The dynamics and simulation of tropical cumulonimbus and squall lines. *Quart. J. R. Met. Soc.*, **102**, 373-394.

Nakazawa, T., 1988: Tropical super clusters within intraseasonal variations over the western Pacific, *J. Meteor. Soc. Japan*, **66**, 777-786.

Nakazawa, T., 1995: Intraseasonal Oscillations during the the TOGA COARE IOP, *J. Meteor. Soc. Japan*, **73**, (special edition), 305-319.

Nicholls, Melville E., Roger A. Pielke and William R. Cotton: Thermally forced gravity waves in an Atmosphere at Rest. *J. Atmos. Sci.*, **48**, 1869-1884.

Numaguti, A., R. Oki, K. Nakamura, K. Tsuboki, N. Misawa, T. Asai, Y. Kodama, 1995: 4-5 day-period variation and low-level dry air observed in the equatorial western Pacific during the TOGA COARE IOP. **73**, (special edition), 267-290.

Pandya, Rajul, Dale Durran and Chris Bretherton, 1993: Comments on "thermally forced gravity waves in an atmosphere at rest." /fI J. Atmos. Sci., **50**, 4097-4101.

Sarachik, E. S. 1985: A simple theory for the vertical structure of the tropical atmosphere. *Pure and Appl. Geophysics*, **123**, 261-271.

Takayabu, Y., 1994: Large-scale cloud disturbances associated with equatorial waves. Part II: Westward-propagating inertio-gravity waves, *J. Meteor. Soc. Japan*, **72**, 451-465.

TOGA COARE International Project Office, 1993: TOGA COARE Intensive Observing Period Operations Summary, June 1993. TOGA COARE International Project Office, UCAR, Boulder, CO.

Young, George S., Samuel M. Perugini, and C. W. Fairall, 1995: Convective wakes in the equatorial western Pacific during TOGA. *Mon. Wea. Rev.,* **123,** 110-123.

Webster, Peter J. and Roger Lukas: TOGA COARE: The coupled ocean-atmosphere response experiment, *Bull. Amer. Meteor. Soc.,* **73,** 1377-1416.